9 Seismic Wave Attenuation: Energy Dissipation in Viscoelastic Crystalline Solids

Reid F. Cooper

Department of Materials Science and Engineering
University of Wisconsin–Madison
Madison, Wisconsin 53706

INTRODUCTION

Seismic imaging as a tool to understand the structure and, perhaps, the dynamics of the planet at depth involves the spatially resolved, combined study of wave velocities and velocity dispersion, wave birefringence and wave attenuation (mechanical absorption). When integrated with insights from petrology, plus-or-minus input from magneto-tellurics, specific hypotheses concerning structure at depth can be formulated (cf. Karato 1993; Karato and Karki 2001). The recent advances in tomography have allowed significant improvements in spatial resolution which also have allowed ever more exacting hypotheses of structure to be articulated. Nevertheless, as is nicely illustrated by the relatively recent seismic analyses of an accreting plate margin (the East Pacific Rise —e.g., Toomey et al. 1998; Webb and Forsyth 1998), the structures inferred at depth can vary significantly: clearly, the interpretation of seismic data is limited specifically by a lack of understanding of the physical processes by which low-frequency wave absorption occurs, particularly in the cases (a) where melt is present and/or (b) where the material is being actively plastically deformed.

This chapter emphasizes the mineral physics/materials science of mechanical absorption, specifically in dense materials at elevated temperature; the interest, then, is in employing the physical study of mechanical absorption to understand natural phenomena such as those mentioned above. Beyond questions of the basic mineral physics of absorption, the guiding interest the community of scholars pursuing the ideas is in isolating actual absorption mechanisms operative in the geological setting thereby allowing for a greater discrimination in the interpretation of seismic data.

At the outset, I note that this contribution does not seek to be a comprehensive review of the ideas and work involved in the physics of mechanical absorption. There are marvelous reviews in the literature that are both authoritative and current; I refer to these frequently in contemplating my own experimental work and so am pleased to point them out here. In the geophysics literature, Karato and Spetzler (1990) have extensively reviewed the variety of lattice-defect-based mechanical loss mechanisms described theoretically in the physics and materials science communities, with an eye towards their application to minerals, while Jackson (1993, 2000) reviewed experimental approaches geared to study these effects in mineral systems. In the materials science literature, the text by Nowick and Berry (1972) remains the standard. In the mechanics literature, the books by Findley et al. (1976; corrected and republished 1989) and, recently, by Lakes (1999) accurately tie down the phenomenology of attenuation. Additionally, in that all of the above authors point out the importance of grain boundaries and solid-state phase boundaries in effecting attenuation (at least in part), Kê's (1999) recent review of a half-century of his own work in the area is significant.

LINEAR VISCOELASTICITY: A CHEMICAL KINETICS PERSPECTIVE

The mechanical properties of solids are distinctly time dependent. When a deviatoric-stress thermodynamic potential is applied to a solid system initially at

1529-6466/00/0051-0009$05.00

mechanical and chemical equilibrium, that system responds—specifically in the form of strain—in a manner that minimizes the new potential: LeChatlier's principle holds in mechanical properties as well as in thermochemistry. (From this point forward, I will refer to the deviatoric stress potential as the "stress potential" or simply the "stress;" "mechanical potential" is used in most thermodynamics treatises to describe pressure, which, of course, must incorporate the hydrostatic component of the applied tensorial stress. Further, hydrostatic pressure can effect mechanical absorption, too: the melt-migration absorption response of partial melts being one example.) The responses to the stress potential combine elastic and inelastic phenomena; the resultant behavior overall is labeled "viscoelasticity." Elastic response, i.e., strain in the form of the stretching and bending of atomic bonds, is considered instantaneous or time-independent (to first order, i.e., ignoring inertial effects). In contrast, inelastic responses are distinctly time dependent: in fully crystalline solids, they involve the interaction of the stress potential with point (vacancies, interstitials, substitutionals, as well as jogs and kinks on dislocations), line (dislocations) and planar (twin boundaries; grain and phase boundaries) lattice defects. Time dependence is a manifestation that the strain so produced involves the motion of these lattice defects: the motion involves the breaking and reforming of atomic bonds, the rate of which is dictated by Boltzmann statistics (and, thus, the rate depends exponentially on temperature). One can further divide inelastic responses, identifying those that produce time-dependent but fully recoverable strain ("anelastic") and those that produce time-dependent, permanent (irrecoverable, "plastic") strain. In that viscoelasticity combines elastic and inelastic responses, viscoelasticity is time dependent.

From a thermodynamics perspective, one understands elasticity as a reversible process where strain energy (i.e., the energy manifest as the distortion of bonds) is stored in the material and is recoverable without loss, while inelastic response is irreversible: strain energy is dissipated within the material, that is, it is converted irreversibly to heat. (Of course, if fracture is initiated, strain-energy dissipation sees the formation of new surfaces as well as the conversion to heat. This chapter, though, will not consider fracture behavior.) Kinetics enters the discussion—and dominates much of the consideration of mechanical response—when (i) temperature is sufficiently high and/or (ii) the application of a deviatoric stress sufficiently slow and/or (iii) the deviatoric stress persists for a sufficiently long time such that either (a) the inelastic strain response(s) occurs at a rate(s) competitive to the elastic response or (b) the accumulated strain produced by the inelastic responses outstrips that from the elastic response.

The elastic and many inelastic responses of materials act in "parallel" kinetically, meaning the responses to stress are independent physically and, as such, the strain produced by each response is additive. Inelastic responses, however, often involve a number of "serial" kinetic steps, which are physical processes that must act in sequence in order to produce strain. Some series-process phenomena are inherent in the process physics (e.g., solution-precipitation—or pressure-solution—creep involves the serial physical steps of (i) atomic dissolution into the liquid phase, (ii) atomic/ionic transport through the liquid phase and (iii) precipitation from the liquid phase; dislocation creep involves the serial process of climb (or cross-slip) and glide of the lattice dislocations), while others are based on geometrical constraints (e.g., diffusional creep acts in series with the processes of grain boundary sliding). The distinction between parallel and serial kinetic processes in mechanical response is important: for a given set of thermodynamic potentials—pressure, temperature, various chemical potentials (e.g., water fugacity, oxygen fugacity, oxide chemical potentials, etc.), and deviatoric stress—and microstructure parameters (e.g., grain size, phase percolation, etc.), the parallel kinetic

mechanism that produces strain most rapidly will dominate the overall mechanical response, while the slowest serial step of that fastest parallel process will rate-limit the response. The major challenge in experimental geophysics is to understand the ranges of thermodynamic potentials giving rise to various mechanical responses in the laboratory time frame, and, also, to understand well the physics of their extrapolation: one must study in the laboratory the same physical process active in the geological environment for the data to be applicable (Paterson 1976). This point is as true for the phenomenon of seismic-frequency mechanical absorption as it is for large-strain creep phenomena.

The maximum strains involved in wave attenuation are quite small, generally $<10^{-6}$ (e.g., Romanowicz and Durek 2000; Karato and Spetzler 1990); correspondingly, the deviatoric stresses involved are small as well, ~10–100 kPa. In this regime, the viscoelasticity in crystalline matter is found to be linear, which means, specifically, two qualities characterize the mechanical behavior: (i) the magnitudes of the strain response and of its first time derivative are directly proportional to the magnitude of the applied stress (e.g., $\varepsilon, \dot{\varepsilon} \propto \sigma^1$, where ε is strain, σ is deviatoric stress and the superposed dot represents a time derivative) and (ii) the rules of mechanical (Boltzmann) superposition hold (e.g., Findley et al. 1976, p.5). Superposition means that the elastic and the (perhaps many) plastic and anelastic responses can be simply summed to discern the overall mechanical response. Superposition is important in understanding how models of dynamic mechanical response are formulated, as will be discussed below.

Wave attenuation arises due to inelastic behavior. It is useful to consider inelastic responses as the relaxation of elastic strain energy: with the application of stress, elastic energy is stored into the material (the "system") instantaneously; inelastic, time-dependent relaxation can then occur, assuming the applied stress is sustained for sufficient time. Behavior can be easily contemplated by considering the system response to two loading approaches. (1) If a fixed amount of strain is applied instantaneously, and then the system is maintained at this strain, the system will experience a relaxation of the stress—and, thus, of the elastic strain energy, which is proportional to the product of stress and strain—until the energy is fully dissipated. In nature, the simplest strain-energy-relaxation function seen—and fairly frequently (e.g., chemical diffusion in a fixed potential gradient; cf. Nowick and Berry 1972, Chapter 8)—is that involving an exponential decay, i.e.,

$$U(t) = U_0 \exp(-t/\tau_R), \tag{1}$$

where U is strain energy (with U_0 being its value after application of the instantaneous stress), t is time and τ_R is the relaxation time, i.e., that time where the energy is decreased to 1/e of its initial value. Lakes (1999, Eqn. 2.6.1) describes the *effective*, time-dependent Young's modulus with this function: if one defines Young's modulus (1-D) as $E = \sigma/\varepsilon$, the stress relaxation means that the modulus apparently decays with time. Alternatively, (2) if the stress step is applied instantaneously and then that stress is maintained, the system will experience flow. The strain energy stored in the material will remain constant, but mechanical energy will be dissipated through the specimen as strain is accumulated. This behavior—flow at constant stress—is called creep; phenomenologically, the system appears to have a time-dependent compliance, J, i.e. (cf. Lakes 1999, Eqn. 2.6.2),

$$J(t) = J_0(1 - \exp[-t/\tau_C]), \tag{2}$$

where τ_C is the characteristic creep or retardation time and, similar to Equation (1), the subscript "0" being the initial value after application of the stress step.

SPRING AND DASHPOT MODELS OF VISCOELASTICITY

In linear mechanical response, exponential "response" functions like Equations (1) and (2) can be modeled using combinations of discrete elastic elements (Hookean springs) and plastic elements (Newtonian-viscous "dashpots"); various of these elements can be arrayed in serial-kinetic or parallel-kinetic form to replicate the mechanical behavior of a system. It is useful for the non-specialist to be exposed to the use of spring-dashpot models because these models often dominate the thinking of mechanics and materials experimentalists and theoreticians—for both good and ill. Before presenting the basic ideas, then, two admonitions are offered. The first—because it is so exacting—is directly quoted from Lakes (1999, p.23):

> *Warning*. Spring-dashpot models have a pedagogic role; however, real materials in general are not describable by models containing a small number of springs and dashpots. (The emphasis is Lakes'.)

Lakes makes this warning because many investigators tend to cling too tightly to exponential-decay, spring-dashpot models as describing exactly some experimental results. The second admonition concerns the relationship between the chemical-kinetics description and the mechanics description—as represented by spring-dashpot models—of mechanical response. Independent physical responses, described above as "parallel-kinetic," end up being portrayed as spring and dashpot elements arranged in series; correspondingly, dependent, "serial-" or "series-kinetic" physical processes translate to springs and dashpots arranged in parallel. In what follows, then, I will carefully distinguish, e.g., "mechanical parallel" from "parallel-kinetic," etc.

Figure 1a presents the spring-dashpot model where one spring (with spring constant R_1) plus one dashpot (with Newtonian viscosity η_1) are arranged in mechanical series; this construct is historically known as the Maxwell Solid model. The response functions corresponding to the constant stress and constant strain conditions mentioned previously are shown as well. One sees clearly that the total strain and strain rate in the Maxwell Solid are the sums of those provided by the spring and the dashpot (i.e.,

$\varepsilon = \varepsilon_1 + \varepsilon_2$ and $\dot{\varepsilon} = \dot{\varepsilon}_1 + \dot{\varepsilon}_2$,

where, in this 1-D model with normal stresses and strains, R_1 will be equivalent to Young's modulus and η_1 to a normal viscosity) and that the elastic and plastic elements respond independently to the stress (i.e., they are kinetically parallel). Release of the stress sees instantaneous recovery of the strain in the spring, but no strain recovery of the dashpot: the Maxwell Solid displays no anelastic behavior. The Maxwell Solid response functions are easily contemplated by considering the strain rate:

$$\dot{\varepsilon} = \dot{\varepsilon}_1 + \dot{\varepsilon}_2 = (\dot{\sigma} / R_1) + (\sigma / \eta_1); \tag{3}$$

thus, the constant-stress (creep) response is

$$\varepsilon(t) = (\sigma_0 / R_1) + (\sigma_0 / \eta_1)t, \tag{4}$$

and the constant-strain, stress-relaxation response is

$$\sigma(t) = \sigma_0 \exp(-R_1 t / \eta_1) = R_1 \varepsilon_0 \exp(-R_1 t / \eta_1). \tag{5}$$

Comparison of Equations (5) and (1) reveals that $\tau_R = \eta_1/R_1$, i.e., 1/e (~37%) of the stress is relaxed in this time.

Placing a spring and dashpot in mechanical parallel results in the Voigt/Kelvin Solid model (Fig. 1b). Here, one sees that the application of step-function (tensile) stress does not see the instantaneous extension of the spring; rather, the spring is loaded/extended at a rate dictated by the viscous-flow extension of the dashpot. Upon release of the stress,

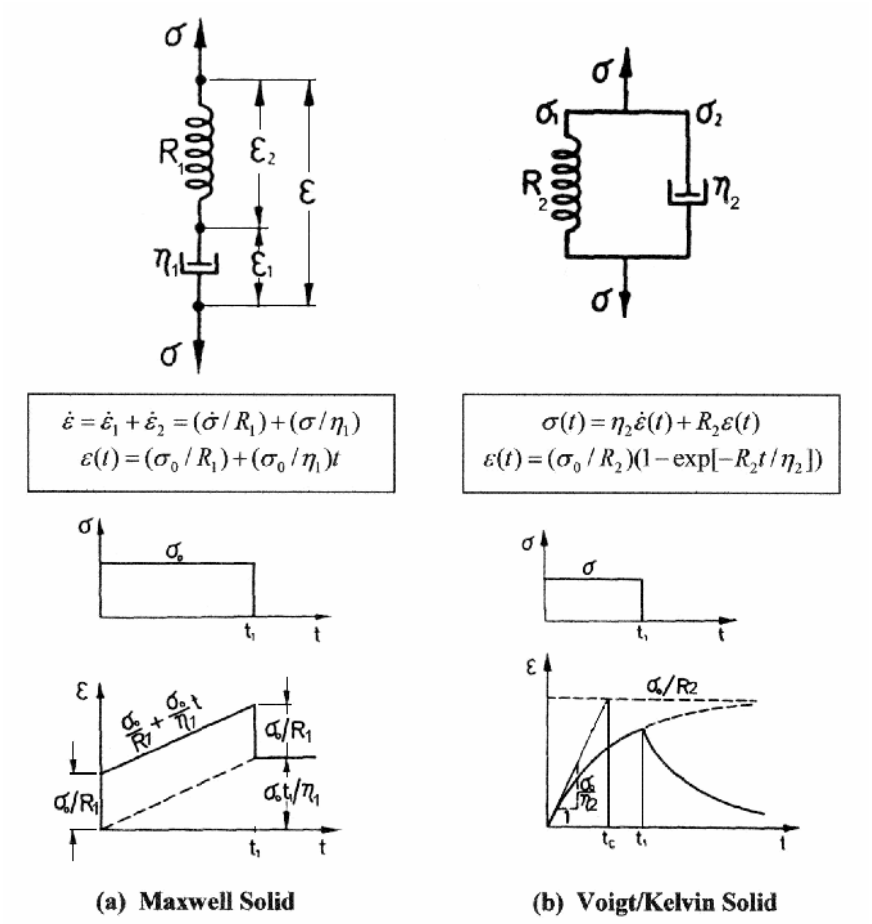

Figure 1. Simple, two-element spring-and-dashpot models of linear viscoelastic solids, including characteristic differential equations and strain responses for static loading. (a) Maxwell Solid. (b) Voigt/Kelvin Solid.

the spring relaxes, again dictated kinetically by the dashpot. The model describes plainly a serial-kinetic process for the accumulation and relaxation of strain. Further, the Voigt/Kelvin Solid is clearly anelastic. In that the responses of the elements are dependent, the Voigt/Kelvin Solid is best considered by considering the constitutive relation between stress and strain:

$$\sigma(t) = \eta_2\dot{\varepsilon}(t) + R_2\varepsilon(t)\,. \tag{6}$$

The creep function for the Voigt/Kelvin Solid is

$$\varepsilon(t) = (\sigma_0/R_2)(1-\exp[-R_2t/\eta_2])\,, \tag{7}$$

and, if the stress is removed from the system at $t = t_1$, the creep function for $t > t_1$ is

$$\varepsilon(t) = \varepsilon_{t=t_1}\exp[-R_2(t-t_1)/\eta_2]\,. \tag{8}$$

For the Voigt/Kelvin Solid, one sees that $\tau_C = \eta_2/R_2$.

Neither the Maxwell or Voigt/Kelvin Solid models, in themselves, accurately model real, viscoelastic solids: the Maxwell Solid has no anelastic behavior and, as such, could not produce the transients seen in plastic flow; the Voigt/Kelvin Solid cannot produce instantaneous strain, nor plastic flow, nor the rather high-rate transients associated

with primary creep. Superposition of these linear models, however, can demonstrate "complete" viscoelastic behavior. The simplest of these compound models is the Burgers Solid, created by arranging the Maxwell and Voigt/Kelvin Solid models in mechanical series (Fig. 2). From the illustration, it is clear that an applied stress allows the two elements of the Maxwell Solid to strain independently of the Voigt/Kelvin Solid and of each other (a parallel-kinetic response), while serial-kinetic behavior of the Voigt/Kelvin solid remains. The creep function of the Burgers Solid model is simply the sum of Equations (4) and (7), or:

$$\varepsilon(t) = (\sigma_0 / R_1) + (\sigma_0 / R_2)(1 - \exp[-R_2 t / \eta_2]) + (\sigma_0 / \eta_1)t\,, \tag{9}$$

where the three terms represent the elastic, anelastic and plastic components, respectively, of the model. The ε vs. t curve for creep in Figure 2 shows, too, the strain response after removal, at time t_1, of the applied stress σ_0: the elastic strain from the Maxwell Solid spring is recovered instantly, the strain from the Maxwell Solid dashpot ceases but experiences no recovery and the anelasticity of the Voigt/Kelvin Solid gives back its strain over time; the creep function for $t > t_1$ is (cf. Eqn. 8):

$$\varepsilon(t) = (\sigma_0 / R_2)(\exp[-R_2 t_1 / \eta_2] - 1)(\exp[-R_2 t / \eta_2]) + (\sigma_0 / \eta_1)t_1\,. \tag{10}$$

One can differentiate Equation (9) to determine strain rate in a continuing creep experiment at stress, σ_0, i.e.,

$$\dot{\varepsilon}(t) = (\sigma_0 / \eta_2)(\exp[-R_2 t / \eta_2]) + (\sigma_0 / \eta_1)\,. \tag{11}$$

The function can be evaluated at very short, but finite time to discern an initial strain rate: $\sigma_0[(1/\eta_2) + (1/\eta_1)] = \tan\alpha$ in the figure; evaluating the function at long time sees that it asymptotically approaches $\sigma_0/\eta_1 = \tan\beta$. In curve-fitting the Burgers Solid model to

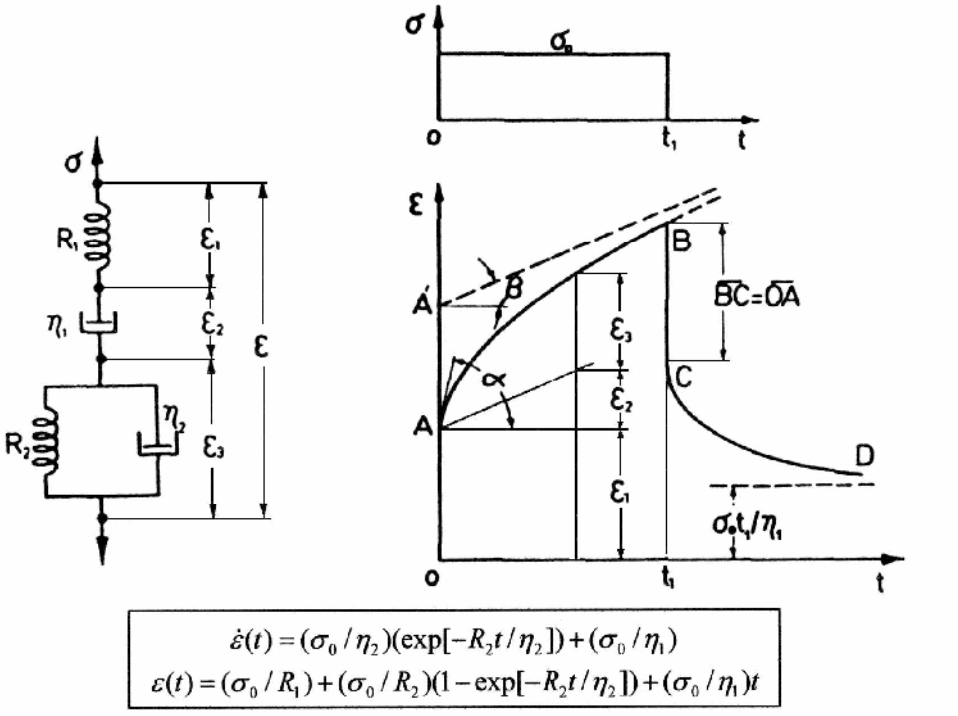

$$\dot{\varepsilon}(t) = (\sigma_0 / \eta_2)(\exp[-R_2 t / \eta_2]) + (\sigma_0 / \eta_1)$$
$$\varepsilon(t) = (\sigma_0 / R_1) + (\sigma_0 / R_2)(1 - \exp[-R_2 t / \eta_2]) + (\sigma_0 / \eta_1)t$$

Figure 2. Burgers Solid (four-element) model, including characteristic differential equation and strain response for static loading/unloading.

high-temperature, Newtonian (diffusional) creep data (of polycrystalline material), the fit is usually dominated (not surprisingly) by the steady-state (long-time) portion of the data; what is learned is that the initial strain rate is invariably underestimated by this simple model. (This behavior will be demonstrated with some real data below.) Nevertheless, the lessons the Burgers Solid model teaches regarding attenuation remain valuable.

ATTENUATION AND THE LINEAR VISCOELASTIC MODELS

Dynamic mechanical response is often described by the "quality factor," Q, which is the ratio of the elastic energy stored to that dissipated. Q is unitless. Attenuation is Q^{-1}, and is further characterized by the nature of loading: the subscript E, G (or μ) or K is applied to discriminate Young's-modulus, shear-modulus or bulk-modulus loading modes, respectively. High-Q (low Q^{-1}) materials are said to "ring," that is, a resonant vibration sees little decay in amplitude for many, many cycles; alternatively, low-Q materials are "lossy," i.e., resonant vibrations decay rapidly. Under ambient conditions, aluminum alloys are high-Q—e.g., $Q \sim 5000$ ($Q^{-1} \sim 2\times10^{-4}$) for a 440 Hz tuning fork—while, by comparison, an identical fork made from wood is quite lossy, vibrating at ~300 Hz and displaying a $Q \sim 33$ ($Q^{-1} \sim 0.03$) (e.g., Lakes 1999, Ch. 7). For very lossy materials ($Q^{-1} > 0.1$), the physical meaning of Q^{-1} is poorly defined. The most common definition is

$$Q^{-1} \equiv (1/2\pi)(\Delta\Phi / W_{\mathrm{MAX}}), \tag{12}$$

where $\Delta\Phi$ is the elastic energy dissipated per cycle of harmonic loading and W_{MAX} is the maximum stored energy per cycle (e.g., Nowick and Berry 1972, p.22; cf. O'Connell and Budiansky 1978). If one considers application to a system of a cyclical stress, i.e., $\sigma = \sigma_0 \cos(\omega t)$, where (now) σ_0 is the stress amplitude and ω is the angular frequency (i.e., the frequency in Hz is $f = \omega/2\pi$), this definition of Q^{-1} is equivalent to the tangent of the phase angle, δ, by which the strain lags the applied stress (i.e., $Q^{-1} \equiv \tan\delta$ and, relative to the stress, the strain is given by $\varepsilon = \varepsilon_0 \cos(\omega t - \delta)$). (In subresonant attenuation measurements, it is δ that is measured directly (e.g., Jackson 1993).) Further, one sees that the viscoelastic modulus (and the viscoelastic compliance) of the system is a complex number, and so it can be demonstrated (e.g., Findley et al. 1976, p.93) that Q^{-1} equals the ratio of the imaginary component of the modulus (termed the "loss modulus") to the real component of the modulus (the "storage modulus").

With these definitions in mind, one can imagine interrogating the Maxwell, Voigt/Kelvin and Burgers Solid models with a cyclic stress function (instead of the static creep function shown in Figs. 1 and 2), and from the responses determine the attenuation spectrum (i.e., Q^{-1} vs. f, which is usually plotted as log Q^{-1} vs. log f) for each model. Given the forms of the differential equations describing the time-dependence of strain rate for the models, these can be Laplace-transformed to discern the frequency response. Table 5.1 in Findley et al. (1976) is a nice presentation of the calculations involved. In short, the Maxwell Solid model produces $Q^{-1} = R_1/(2\pi f \eta_1) = 1/(2\pi f \tau_R)$, which is a straight line with slope –1 on a log Q^{-1} vs. log f plot. Alternatively, the Voigt/Kelvin Solid model produces $Q^{-1} = (2\pi f \eta_2)/R_2 = 2\pi f \tau_C$, a straight line with slope +1 on a log Q^{-1} vs. log f plot. For the Burgers Solid model, the form of $Q^{-1}(f)$ is significantly more complex:

$$Q^{-1} = \frac{p_1 q_2 \left[2\pi f\right]^2 + \eta_1\left(1 - p_2\left[2\pi f\right]^2\right)}{p_1\eta_2\left[2\pi f\right] - q_2\left[2\pi f\right]\left(1 - p_2\left[2\pi f\right]^2\right)} \tag{13}$$

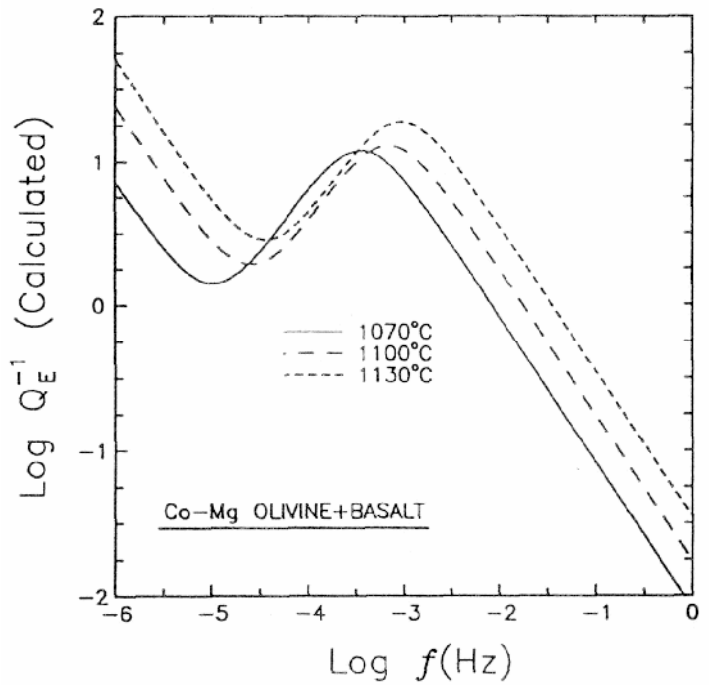

Figure 3. Dynamic response of the viscoelastic Burgers Solid model. The curves shown are for an analytical Laplace inversion of the Burgers model being first fit to experimental, flexural creep response of a Co-Mg olivine-basalt partial melt The characteristic attenuation response of the Burgers Solid includes a Debye peak related to the anelastic (Voigt/Kelvin) element. [Used by permission of American Geophysical Union, from Green et al. (1990) *Geophysical Research Letters*, Vol. 17, Fig. 4, p. 2099.]

where

$$p_1 \equiv (\eta_1 / R_1) + (\eta_1 / R_2) + (\eta_2 / R_2), \tag{14}$$

$$p_2 \equiv (\eta_1 \eta_2) / (R_1 R_2), \text{ and} \tag{15}$$

$$q_2 \equiv (\eta_1 \eta_2) / R_2. \tag{16}$$

The form of the Burgers Solid absorption spectrum is illustrated in Figure 3 (above), in which experimental flexural creep curves—for partially molten, nominally texturally equilibrated, Newtonian-viscous (Co-Mg) olivine-liquid "basalt" aggregates—were first curve-fit (for η_1, η_2 and R_2, with a textbook value used for R_1) to the model (Eqn. 9) and then transformed via Equations (13)-(16) (Green et al. 1990). (The creep experiments, in four-point flexure (Cooper 1990), examine the time-dependent Young's modulus behavior, thus the curves in Figure 3 are for Q_E^{-1} and R_1 equals the temperature-compensated, high-frequency (i.e., unrelaxed) Young's modulus.) The attenuation spectrum for the Burgers Solid shows Q_E^{-1} tending to infinity at low frequency, consistent with domination of energy dissipation by the Maxwell Solid dashpot (steady-state creep response with η_1) under these conditions; at high frequency, the dominant absorption behavior remains the Maxwell Solid dashpot (the spring cannot effect absorption, by definition), and the slope of -1 continues as Q_E^{-1} approaches zero. In an intermediate frequency, one sees that the anelastic Voigt/Kelvin component produces a discrete and pronounced attenuation peak (a Debye peak), with the deviation from the Maxwell Solid model spectrum occurring at $f \sim 1/2\pi\tau_C = 1/(2\pi[\eta_2/R_2])$. One sees that an increase in temperature causes the spectrum, in its entirety, to shift to higher frequency.

The primary temperature effect is on the values of η_1 and η_2, which, following Boltzmann statistics, each depend exponentially on temperature (i.e., $\eta_i \propto \exp(E_{a,i}/RT)$, where E_a is the activation energy for the physical process rate-limiting the viscosity, T is temperature and R is the gas constant). The shift of the anelastic peak to higher f as T increases is not necessarily the same shift as that for the straight-line Maxwell Solid-dominated component of the spectrum in that η_1 might not have the same E_a as does η_2.

Two points require emphasis here, justifying the time spent contemplating the attenuation spectrum produced by Burgers Solid model. First, experimentalists get very excited when a Debye peak, like those that punctuate the spectra shown in Figure 3, appears in their *measured* attenuation data. (Please note: the peaks shown in Fig. 3 were *not* produced in cyclic loading experiments; rather, the peaks shown came from fitting a model—the Burgers Solid model that, by definition, produces a Debye peak when it is transformed—to creep data.) This excitement occurs because the peak's presence suggests operation of an anelastic mechanism that has a unique τ_C, one that can perhaps be proven to correspond to a unique, physical causal mechanism in the material. Examples of Debye-peak behavior include (1) the Snoek relaxation, in which interstitial impurities diffuse from one interstitial site to an empty, adjacent one because an applied stress destroys the potential-energy degeneracy of the interstitial sites (e.g., Nowick and Berry 1972, Ch.9) and (2) the Zener (1941) grain boundary relaxation (seen infrequently) associated with uniform grain-sized aggregates having grain boundaries of nominally identical viscosity in a thermodynamic regime where mechanical energy dissipation is dominated by grain boundary sliding (e.g., Kê 1947, 1999); the review by Karato and Spetzler (1990) covers other mechanisms as well. The materials and mechanics literature on attenuation (or "damping," or "internal friction," if one is contemplating a literature search) has many, many contributions where, if a peak is discovered—even one that might be considered noise—the entire discussion section is dedicated to discerning that unique physical phenomenon giving rise to the peak, while the rest of the experimental spectrum is ignored, that is, simply extracted away as "background."

The second point justifying time on the Burgers Solid model is that the impact of temperature on absorption is better illustrated and thus contemplated. The shift in frequency—and, to first order (at least), not-at-all in height—of the Debye peak with temperature is clearly illustrated in Figure 3 and, thus, understood as the impact of Boltzmann statistics: i.e., as T is increased, the probability of a stress-driven motion of a specific lattice defect occurring within a fixed time increases exponentially. But consider, for example, those portions of the spectra in Figure 3 between $-2.5 \le \log f \le 0$. The power-law form of the data (i.e., $Q_E^{-1} \propto f^m$) in this region produces an array of straight lines (of slope m, which, in this example, happens to be $m = -1$) in the log-log plot. This straight-line form tempts one to think that it is Q_E^{-1} that is exponentially dependent with temperature at constant f. Indeed, in power-law attenuation data for which a Debye peak is not seen—which, as noted below, occurs frequently in high-T experimental materials studies and, too, characterizes, e.g., the absorption response of the upper mantle—this approach to temperature-effect extrapolation/interpretation is often taken, and referenced to Schoeck et al. (1964). For most situations, to do so is to ignore the physics of absorption: Nowick and Berry (1972, p.458) note explicitly that any "effective" activation energy discerned this way has no physical meaning. The frequency shifts with T for the Debye peaks remind us of this fact. Further, in Figure 3, one realizes that the frequency-shift phenomenology must remain true for those portions of the spectra located away from the peak: the Maxwell Solid dashpot represents, in this case, the diffusional (Newtonian) creep of polycrystalline olivine, which is effected by point-defect mechanisms of chemical diffusion.

To be complete, however, one can articulate two physical possibilities for a vertical

shift of a log Q^{-1} vs. log f spectrum with temperature. The magnitude of specific absorption at a fixed frequency is dependent on the spatial density of lattice-defect-based absorbers. If, for entropic reasons, an increase in temperature causes an increase in density of these defects, one can envision an absorption increase as T increases. Most mechanisms of absorption are based on extrinsic defects, however; thus this possibility seems limited. (Indeed, in the case of the extrinsic-defect-effected Snoek relaxation noted above, an increase in T is found to *diminish* the height of the Debye peak: higher T promotes randomization of impurity interstitials, negating the stress-induced loss of degeneracy of interstitial site energy.) The other possibility is that an increase in temperature allows access to a new, and perhaps more potent, absorption mechanism, i.e., a change in the parallel-kinetic mechanism and/or the rate-limiting serial-kinetic process dominating the dynamic behavior. Behavior of this type—i.e., mechanism change with a change in thermodynamic and/or microstructural conditions—can perhaps be inferred from recent experimental attenuation data, as will be presented below.

THE ATTENUATION BAND/HIGH-TEMPERATURE BACKGROUND

Experimental attenuation data seen in most rock and mineral studies, as well as in many studies of engineering materials, do not match well with the simple viscoelastic models described above—which is the basis of Lakes' (1999) warning noted earlier. At high (homologous) temperature, what is usually seen is a power-law absorption, $Q^{-1} \propto f^{m}$, where m is in the range $-0.5 \leq m \leq 0$ over several orders of magnitude in frequency. This response has been referred to at the "attenuation band" or "absorption band" in the geophysics literature; in the materials literature it is known as the "high-temperature background" absorption. Most dramatic of the experimental studies of the high-temperature background in the materials literature is the work of Lakes and co-workers on low-melting-point metals, alloys and intermetallic compounds, where the power-law behavior is noted for up to ten orders of magnitude in frequency ($10^{-5} \leq f[\text{Hz}] \leq 10^{5}$) for, e.g., two-phase mixtures of β-In_3Sn + γ-$InSn_4$ at room temperature, which is ~75% of the β-γ eutectic temperature (Lakes and Quackenbush 1996). The mantle of Earth, too, shows this behavior, where shear-waves demonstrate $Q_G^{-1} \propto f^{-(0.15-0.4)}$ (i.e., $-0.40 \leq m \leq -0.15$; e.g., Anderson and Minster 1979; Anderson and Given 1982; Molodenskiy and Zharkov 1982). Figure 4, from Anderson and Given (1982), shows well the behavior for the mantle, giving both references for the window of frequencies of interest ($10^{-3} \leq f[\text{Hz}] \leq 1$) as well as absolute values of Q^{-1} (10^{-3} to 10^{-2}, although at shallow depths near accreting plate margins, Q_G^{-1} can reach ~0.1—e.g., Chan et al. 1989).

The broad absorption band requires a *distribution* of material compliances. From a perspective that emphasizes solely exponential relaxation processes, this distribution arises from (i) a variety of exponential-decay mechanisms, each with a unique τ_C, that sum to produce the response overall or (ii) a single exponential-decay mechanism in which a variation of a spatial component, e.g., grain size, allows for a variety of τ_C's or (iii) some combination—probably complex—of both. Mechanistically, one can apply the exponential-decay, linear viscoelastic models to experimental data so as to discern whether a discrete number of Voigt/Kelvin elements of differing τ_C might match well the data. Schematically, the idea is presented in Figure 5, which compares a "Multiple (Voigt/)Kelvin" approach to the Burger's Model.

Figure 6 presents some experimental creep data (Fig. 6a,c,e; the same data are in each figure) and experimental attenuation data (Fig. 6b,d,f; again, the same data are in each figure) for an enstatite glass-ceramic. This material is composed of 95 vol % of a very uniform, 0.5-μm grain-sized (ortho)enstatite (with some clinoenstatite intergrowths, though insufficient in volume to perceive in X-ray diffraction) with 5 vol % of a residual sodium-magnesium aluminosilicate glass, confined to grain triple junctions—a model

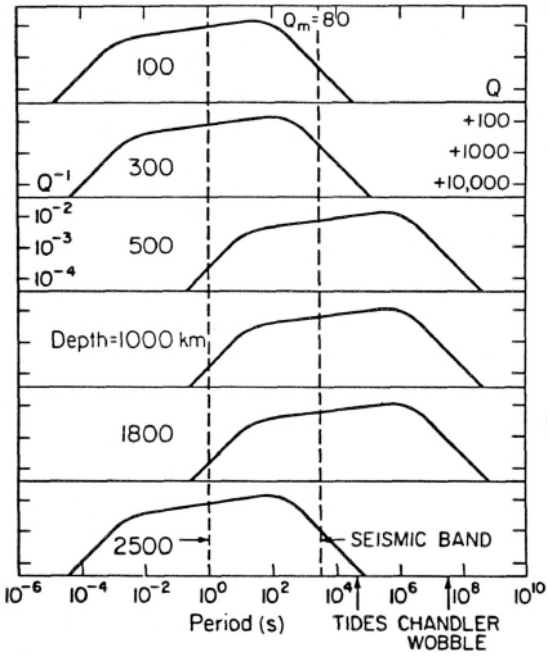

Figure 4. Absorption band model of Earth's mantle: Q (and Q^{-1}) vs. wave period ($\equiv f^{-1}$) and depth. [Used by permission of American Geophysical Union, from Anderson and Given (1982) *Journal of Geophysical Research*, Vol. 87, Fig. 3, p. 3896.]

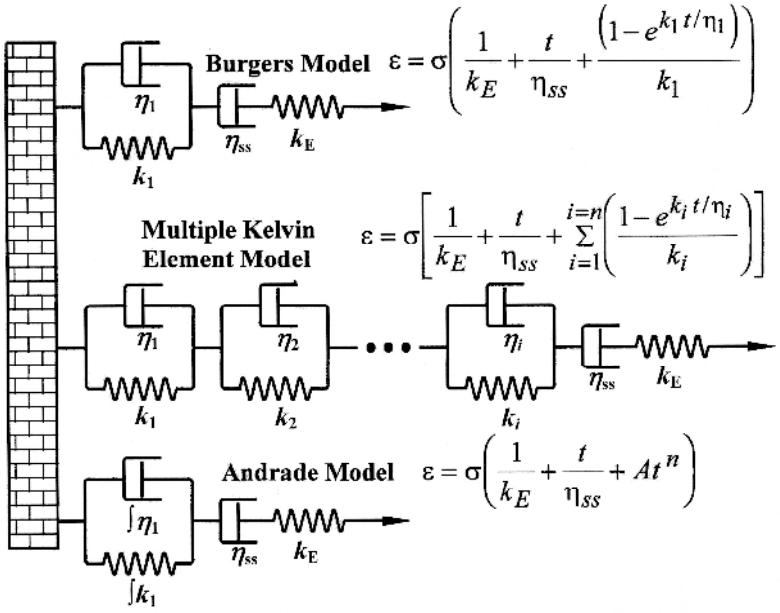

Figure 5. Alternative viscoelastic models—and their respective strain responses—to compare with the Burgers Solid model. The Multiple (Voigt/)Kelvin model employs discrete exponential-decay elements with unique τ_C's that superpose to estimate a power-law absorption response. The Andrade model assumes a continuous distribution of compliances, which can represent either many exponential-decay elements or one or more non-exponential-decay relaxation processes. [Used by permission of Plenum Press, from Gribb and Cooper (1995). In *Plastic Deformation of Ceramics*, edited by R.C. Bradt et al., Fig. 3, p. 91.]

silicate partial melt. (Details of the materials fabrication and its microstructure and thermal/mechanical stability are given in Cooper (1990)). The creep tests were performed in four-point flexure; the attenuation measurements were performed in reciprocating four-point flexure (Gribb and Cooper 1995).) The material, at the temperatures tested, had a

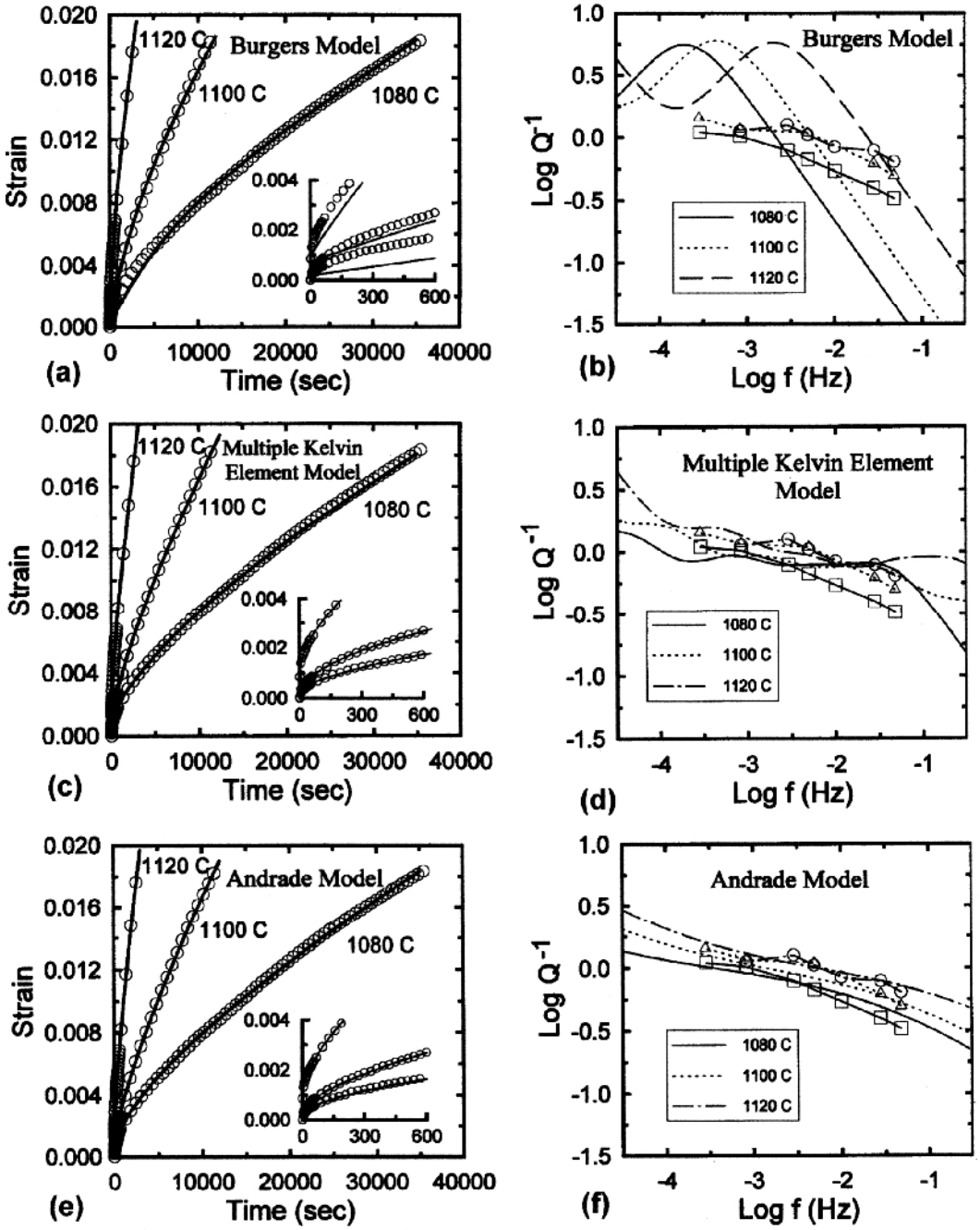

Figure 6. (a),(c),(e) Experimental, unidirectional, four-point flexural creep data (open circles) for an enstatite glass-ceramic (a model partial melt) versus the best fits of the three linear models, respectively, shown in Figure 5 (solid lines). For each graph, the short-time/small-strain response and model fit are shown in the inset. (b),(d),(f) Experimental Q_E^{-1} response for the enstatite glass-ceramic obtained from reciprocating four-point flexure (curves with symbols) versus Q_E^{-1} predictions calculated from numerical inversion of the linear models (curves without symbols). [Used by permission of Plenum Press, from Gribb and Cooper (1995). In *Plastic Deformation of Ceramics*, edited by R.C. Bradt et al., Fig. 5, p. 94.]

Newtonian steady-state viscosity; linearity was proven in both creep and attenuation modes. As shown in the constant-stress creep curves, there is a significant creep transient. This transient was experimentally demonstrated as fully recoverable; it is anelastic. Figures 6a and 6c compare the fit of the Burgers Solid model and of a computer-

arbitrated, Multiple Kelvin Solid model, respectively, to the creep data. ("Computer-arbitrated" means the algorithm selects the number of elements and the τ_C of each following the philosophy articulated by Thigpen et al. (1983); the programmer diminishes the size of discrete time steps available for the τ_C's until the result is unaffected by the size of these steps (Gribb 1992).) Clearly seen in Figure 6a is the Burgers Solid model underestimating the initial strain rate, as was noted earlier. Also evident is the far better fit to the data by the Multiple Kelvin Solid model. All of the Multiple Kelvin Solid fits to these data produced three distinct Voigt/Kelvin elements, which demonstrated appropriate frequency shifts with the changes in temperature studied. These model results are Laplace-transformed and compared to the experimental attenuation data in Figures 6b and 6d; the fits to the creep data are the data-free curves, while the experimental data (points) are connected with discrete line segments. The attenuation data demonstrates clearly the simple power-law spectrum. Equally clear is the inadequacy of the Burgers Solid model to predict the attenuation. (Gribb et al. (1994) measured, too, the Q_E^{-1} response of the Co-Mg olivine-basalt material, and the comparison of those data to the transformed creep curves shown in Figure 3 are qualitatively similar in their poorness of fit.) One sees that the Multiple Kelvin model inversion matches the data far better, but, consistent with its discrete nature, produces three Debye peaks that superpose to closely match the data. The data, in that they appear to vary monotonically with frequency, certainly do not loudly proclaim the adequacy of the "bumpy" Multiple Kelvin model fit, although their resolution could be limiting. Of course, if the fit was better, the problem remains regarding deciding what physical phenomena these discrete Voigt/Kelvin elements represent.

A third curve fit is shown in Figure 6. The Andrade Model is an empirical, phenomenological model, first used to describe the creep of polycrystalline metals:

$$\varepsilon = \sigma[(1/E) + (At^n) + (t/\eta_{ss})], \tag{17}$$

where η_{ss} is the steady-state viscosity, A is a constant and the time exponent n is less than one. (Andrade (1910) explicitly articulated $n = 1/3$ and that η_{ss} could be an effective viscosity, i.e., the steady-state behavior was not limited to Newtonian flow.) In the framework of linear viscoelasticity, the Andrade Model can represent an infinite number of (exponential-decay) Voigt/Kelvin elements possessing a continuous distribution of relaxation times. The match of the Andrade model, both with $n = 1/2$ and with n used as a flexible parameter (the error difference between approaches was negligible), to the creep data is quite accurate, and its transformation matches the attenuation results beautifully; indeed the transformation of the Andrade Model produces a region in the attenuation spectrum where $Q^{-1} \propto f^m$ with $(1-n) \le m \le 0$.

Thus, the materials physics in this case demands reflection. As a creep function that possesses a continuous distribution of compliances, the Andrade Model need not represent an infinite number of linear viscoelastic elements with exponential decay behavior, for other decay functions (e.g., a "stretched" exponential; Lakes 1999, p.326) can be integrated to effect as well. For example, in the cases of the enstatite glass-ceramic (Gribb and Cooper 1995) and the Co-Mg olivine-basalt partial melt (Gribb et al. 1994), the Young's-modulus-mode relaxation could be modeled quite nicely, albeit qualitatively (A in Equation (17) being empirical and overly flexible, for example), as D'Arcy flow of the melt phase across the flexure specimen in response to the gradient in the hydrostatic component of the stress tensor. The melt-migration problem thus resembles chemical diffusion in a potential gradient that diminishes with response, which is a $t^{1/2}$ relaxation and not an exponential one. Convoluted in these data, then, are solid-state effects, some undoubtedly in shear (the Young's-modulus bending experiments convolute shear- and bulk-modulus responses (cf. Green and Cooper 1993)). How should these effects be dealt

with? Further, can one *predict* the magnitude of the attenuation and the shape of the attenuation-band spectrum from a physically sound foundation?

There are lovely data in the literature for melt-free, polycrystalline aggregates tested in both shear creep and subresonant oscillatory shear. In the geophysics literature, the work out of Jackson's laboratory on olivine (e.g., Tan et al. 2001; Jackson et al. 1992, 2002) and on perovskite (Webb et al. 1999) is noteworthy for its attention to detail in specimen preparation and characterization and, particularly—because of the use of high confining pressure in their experiments—for the elimination of grain-boundary cracking, which the rock physics community considered affected negatively ambient-pressure experiments performed earlier (e.g., Berckhemer et al. 1982). In materials and mechanics, the literature is broad, quite extensive—particularly for metals—and of long standing (e.g., the many references in Zener (1948) and Nowick and Berry (1972)), but it is the recent work out of Lakes' lab on various metals/alloys that is provocative because of the large range of frequencies studied and other experimental innovation (e.g., Cook and Lakes 1995; Lakes and Quackenbush 1996; Dooris et al. 1999). The attenuation band behavior is seen in all cases, and, as already noted, for wide ranges of frequency in the case of both polyphase and single-phase polycrystalline metals. Inevitably, then, some of the data in Figure 6 must be attributed to solid-state processes in addition to melt-migration effects.

Perusal of many experimental and observational papers on absorption in crystalline materials, where the data display the attenuation band with no discernable Debye peak(s) superposed, inevitably reveals a qualitative-to-semiquantitative discussion concerning a variation/distribution in defect length scale and its consequent impact to create a distribution in τ_C in the material. Most frequently speculated are variations in grain size and/or variations in the pinning lengths of lattice dislocations (cf. Anderson and Given 1982; Lakes 1999, p.315). And yet, even as models for such broadband absorption become more complicated (e.g., D'Anna et al. (1997) for the case of variation in dislocation pinning length), they so far fail to produce an accurate prediction of the magnitude of Q^{-1} for a given set of thermodynamic and microstructural constraints, nor of the value of m characterizing the attenuation band.

ISOLATION/CHARACTERIZATION OF A SINGLE PHYSICAL MECHANISM PRODUCING A POWER-LAW ATTENUATION SPECTRUM: THE INTRINSIC TRANSIENT IN DIFFUSIONAL CREEP

Gribb and Cooper (1998) set out to characterize the shear attenuation behavior in polycrystalline olivine aggregates that (i) had such a uniform grain size that, to first order, one could analyze as having no grain-size variation, (ii) were prepared with such a fine grain size that no thermal-expansion-anisotropy grain-boundary cracking would occur in the process of heating or cooling the specimens (the experiments were to be performed at ambient pressure) and (iii) were fabricated and mechanically tested under differential-stress conditions that would disallow the nucleation of lattice dislocations. The idea was simple: we desired to get rid of microstructural scale distributions and see what happens to the shear absorption spectrum. The material was prepared by pulverizing Balsam Gap (Jackson Co., NC) dunite to sub-micrometer dust, classify the particle size and "gently" (low-pressure), uniaxially hot-press the material back into a polycrystalline solid. Given the three material qualities noted above, the stress/temperature conditions for hot-pressing were the critical parameter: for a 3-μm grain size aggregate, for example, conservative theory indicated that the hot-press pressure could not exceed 24 MPa at 1200°C if nucleation of lattice dislocations was to be avoided. Further, use of the Balsam Gap material had some advantages: very-fine (≤ 1 μm in the fabricated materials) second

phases of chromite and enstatite (< 1 vol % each) plus impurity Ca^{2+}, which segregates to grain boundaries, succeeded in shutting down grain growth of the dense, 3-μm grain-size aggregates during the mechanical test experiments. Test conditions included a temperature range of 1200–1285°C, maximum torsional shear stresses of 10–120 kPa (with mechanical linearity demonstrated for this range), and frequencies for the reciprocating experiments of $10^{-0.5}$–$10^{-2.5}$ Hz.

The creep curves demonstrated a distinct transient, similar to those seen, e.g., in Figure 6a; these were demonstrated to be fully anelastic. The creep behavior was demonstrated as Newtonian, that is, diffusional deformation dominated the steady-state flow—a result consistent with other studies of olivine under similar thermodynamic conditions (e.g., Karato et al. 1986; Hirth and Kohlstedt 1995). Further, the thermal activation energy for the transient matched that for the steady-state response, indicating their cause by the same physical mechanism. The attenuation data are presented in Figure 7, along with the inversions of the Andrade Model fit to the creep data. Once again, the attenuation-band behavior is discovered ($Q_G^{-1} \propto f^{-0.35}$) and its useful characterization by the inversion of the Andrade Model reconfirmed. Further, the absolute values measured for the of the attenuation, and the behavior in general, are found to be consistent with studies on similar synthetic olivine aggregates measured in Jackson's laboratory at high confining pressure (e.g., Tan et al. 1997, 2001), meaning that, as expected from theory, the fine-grained aggregates have not been affected by grain-boundary cracking. Now, however, one cannot cite a microstructural scale distribution to be the source of a distribution of compliances: the Andrade behavior and the related attenuation band are intrinsic to the diffusional creep mechanism operative in the experiments.

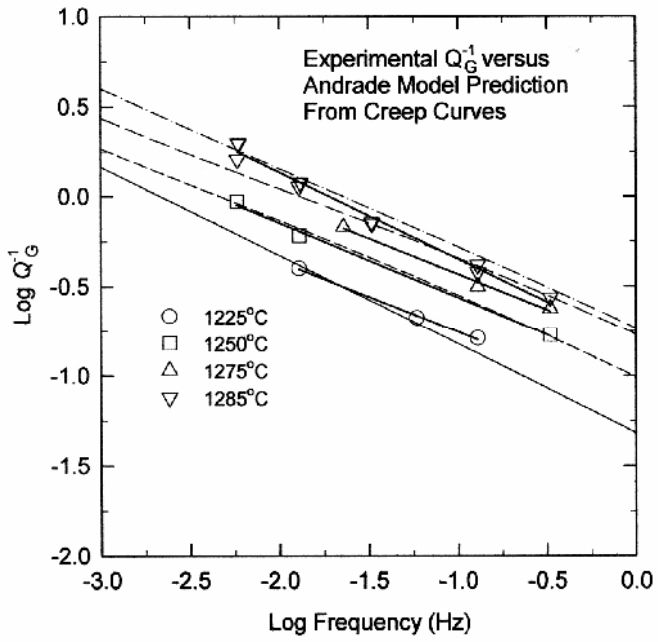

Figure 7. Q_G^{-1} of fine-grained ($d \approx 3$ μm) olivine (Fo_{88}) measured in reciprocating torsion (points with heavy curves) versus that predicted from the Laplace transform of the Andrade-model, best fit (with $n = 1/2$) to the unidirectional torsional creep response (fine curves). [Used by permission of American Geophysical Union, from Gribb and Cooper (1998) *Journal of Geophysical Research*, Vol. 103, Fig. 7, p. 27272.]

Following the theoretical treatments of Lifshits and Shikin (1965) and Raj and Ashby (1971), and then extended by Raj (1975), one discovers that the apparent continuous distribution of compliances is created in the chemical diffusion response that seeks to evolve the stress distribution (normal traction) on grain boundaries from an initial state where singularities exist at grain triple junctions to the steady state that requires the traction be highest in the center of boundaries and near zero at triple junctions. The process is well characterized as chemical diffusion within a diminishing potential; its analysis allows the articulation of a universal creep response and, through its inversion, a universal attenuation spectrum, applicable to all crystalline materials having a Newtonian (diffusional) rheology.

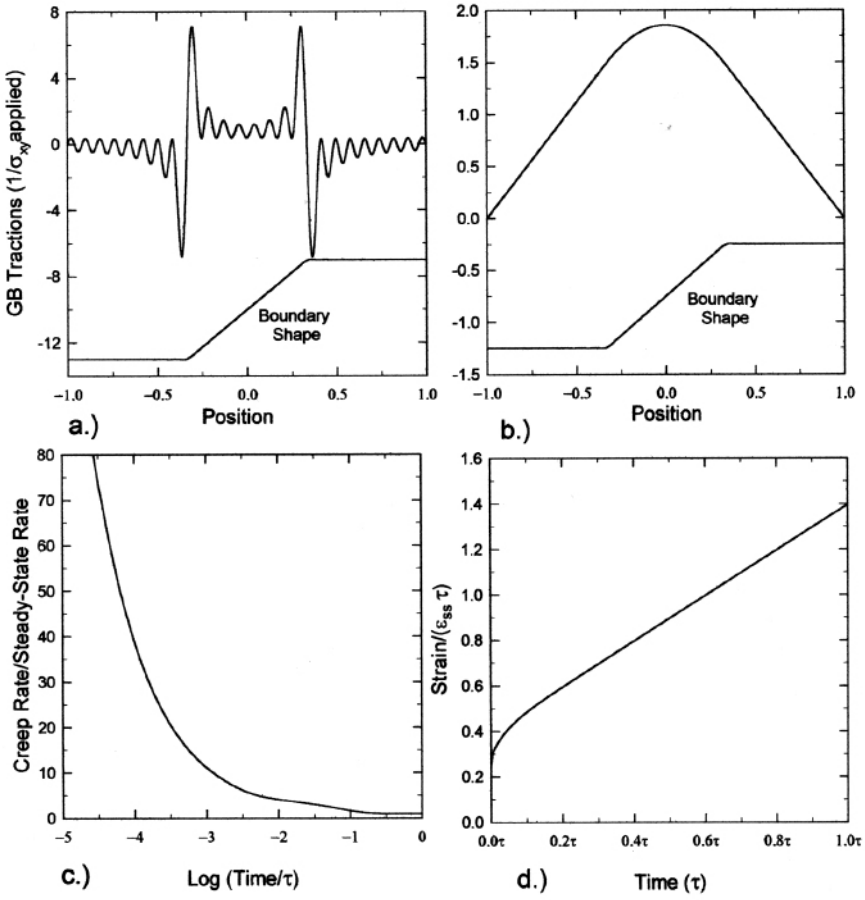

Figure 8. Calculation of a universal creep curve for all polycrystalline materials deforming by grain-boundary-diffusion creep under conditions in which the grain boundaries have no resistance to shear (after Raj 1975). (a) Initial distribution of normal traction on grain boundaries for a 2-D array of hexagonal grains: singularity-like high tractions occur at triple junctions. (The high-frequency oscillations are numerical artifacts due to the Fourier approximation to the stress state.) (b) Traction distribution consistent with a steady-state diffusive flux along grain boundaries (and, thus, a steady-state creep rate). (c) Integrated creep rate (normalized by the steady-state strain rate) from a numerical solution of the diffusion equations (Fick's laws). The characteristic time of the transient, τ, is defined based on the diffusion behavior (Eqn. 18); one sees that 99% of the transient is played out by ~0.25τ. (d) Universal creep curve obtained by integration of the curve shown in (c). One sees that, over the period τ, an additional 60% of inelastic strain is generated over that predicted by the steady-state response. The amount of elastic strain (strain at time zero) is constrained by the model to be ~$(\dot{\gamma}_{ss}\,\tau)/4$. [Used by permission of American Geophysical Union, from Gribb and Cooper (1998) *Journal of Geophysical Research*, Vol. 103, Fig. 8, p. 27273.]

The framework for the model is presented in Figure 8. Diffusional creep is driven by the spatial gradient of normal tractions on grain boundaries and is rate-limited either by diffusion through the crystalline lattice (Nabarro-Herring creep: Nabarro 1948; Herring 1950) or along the grain boundaries (Coble creep: Coble 1963). Material continuity, however, requires that these diffusional mechanisms act in kinetic series with some process of grain boundary sliding (Raj and Ashby 1971; cf. Courtney 1990, p.276). Because of the serial nature of the process overall, there are thermodynamic conditions where grain boundary sliding component essentially dissipates no energy, i.e., conditions where the grain boundaries have no resistance to shearing. It is this situation of boundaries inviscid to shear that is described by Raj (1975), and replicated and extended in Figure 8—for the geometrical case of a 2-D array of hexagonal grains—to produce a "universal" creep curve for diffusional creep. Figure 8a shows the initial stress distribution for the material with inviscid boundaries: traction singularities exist at all triple junctions. The traction distribution consistent with a steady-state diffusion flux, on the other hand, consists of tractions being maximized at the center of grain faces and diminish to zero at the triple junctions, a parabolic distribution in 2-D (Fig. 8b) or paraboloidal in 3-D. Evolution of the traction distribution from that shown in Figure 8a to that in Figure 8b constitutes the intrinsic transient in diffusional creep. One should note that this transient is anelastic: for example, removal of the far-field applied stress after the material has achieved steady state sees an internal stress predicated on the traction distribution in Fig 8b that will be relieved by diffusion, giving strain recovery. One can solve Fick's 2nd law for the evolution of the tractions from the initial to the steady-state conditions to calculate the transient (Fig. 8c) and then integrate this function to discern a universal creep curve (Fig. 8d). Finally, this creep curve can be transformed to an attenuation spectrum.

This "universal" attenuation spectrum is presented in Figure 9. The single mechanism produces an attenuation-band response, though three regions of isothermal behavior are noted: (i) at low frequency, Q^{-1} is dominated by the steady-state creep response, producing $Q^{-1} \propto f^{-1}$ (cf. the Maxwell Solid model); (ii) at high frequencies, the elastic contribution to the total strain becomes dominant and $Q^{-1} \propto f^{-0.5}$; and (iii) at intermediate frequencies the anelastic transient dominates behavior, with $Q^{-1} \propto f^{-(0.25-0.4)}$. One sees that the creep and attenuation response is scaled by a characteristic relaxation time τ, which, for the case of a grain-boundary-diffusion-effected Newtonian rheology, is given by (for the simplified, 2-D hexagonal grain model)

$$\tau = \frac{3\sqrt{3}\left(1-\nu^2\right)d^3 \mathrm{k}T}{2\pi^3 E\, D_\mathrm{b}\, \xi\Omega} \quad , \tag{18}$$

where ν is Poisson's ratio, d is the grain size, E is Young's modulus, D_b is the grain boundary diffusion coefficient for the rate-limiting ionic species, ξ is the characteristic grain boundary width, Ω is the molecular volume, and kT has the usual meaning. Please note: this τ is not to be confused with the standard period ascribed to an exponential decay process in a linearly viscoelastic solid; rather, τ is a non-exponential relaxation associated with chemical diffusion within a diminishing potential gradient: with application of stress, e.g., in a creep test, the strain rate decays to within 1% of the steady-state value by ~0.25τ. One sees a power-law grain-size dependence of τ: the value 3 for this exponent follows the grain-boundary diffusion model. The steady state strain rate calculated for this same, 2-D model is (Raj and Ashby 1971; cf. Coble 1963):

$$\dot{\gamma}_\mathrm{ss} \cong \frac{132\,\sigma_\mathrm{xy}\,\Omega\,\xi D_\mathrm{b}}{\mathrm{k}T\,d^3} = \frac{\sigma_\mathrm{xy}}{\eta_\mathrm{ss}} \quad , \tag{19}$$

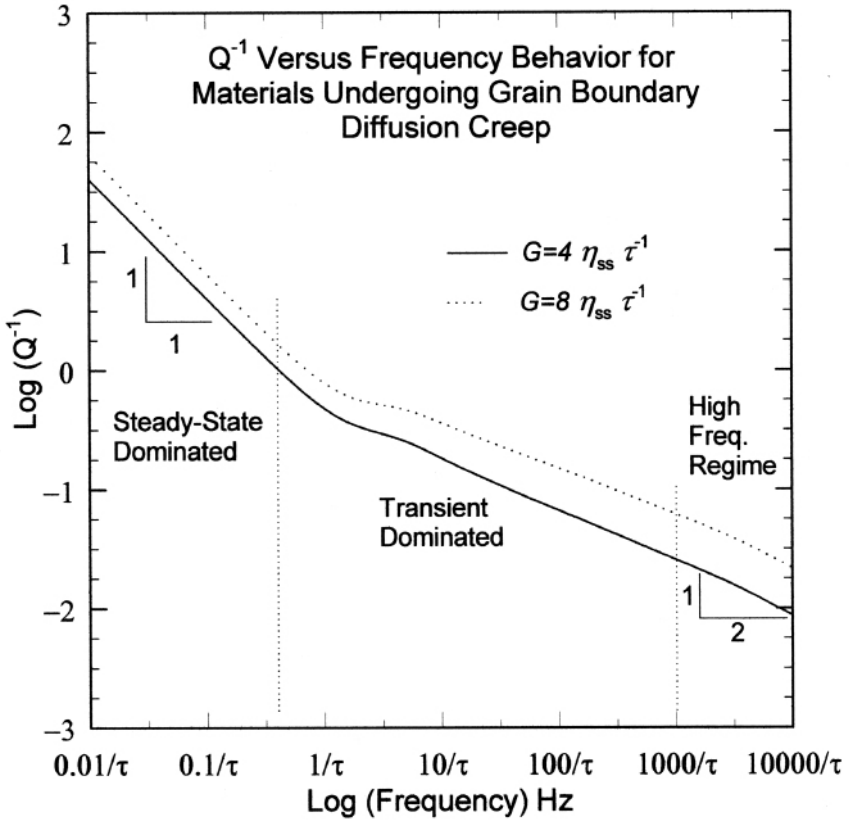

Figure 9. Universal Q^{-1} versus frequency curve for all materials deforming via grain boundary diffusional creep, predicted by numerical Laplace transform of the creep curve shown in Figure 8d. The Q^{-1} behavior displays three distinct regions of behavior: (i) at low frequencies, steady-state dominates and $Q^{-1} \propto f^{-1}$; (ii) at intermediate frequencies, the transient interacts with the steady-state response and $Q^{-1} \propto f^{-(0.25-0.4)}$; (iii) at high frequencies, the elastic behavior interacts with the transient response and $Q^{-1} \propto f^{-0.5}$. The simplifications inherent in the formulation (e.g., geometry) may result in an error on the order of a factor of two. The effect of such an error is illustrated by the dotted line that represents the attenuation behavior of the model with a reduced modulus or, equivalently, an increased steady-state creep rate. [Used by permission of American Geophysical Union, from Gribb and Cooper (1998) *Journal of Geophysical Research*, Vol. 103, Fig. 9, p. 27274.]

where $\dot{\gamma}_{ss}$ is the steady state shear strain rate and σ_{xy} is the applied, far-field shear stress. By combining Equations (18) and (19), and assuming that $\nu = {}^1/_3$, τ is defined in terms of the steady state response:

$$\tau \cong \frac{10\sigma_{xy}}{E\dot{\gamma}_{ss}} = \frac{10\eta_{ss}}{E} \cong \frac{4\eta_{ss}}{G} . \tag{20}$$

Simply stated, for an aggregate that deforms by diffusional creep, knowing the steady-state viscosity and the temperature-affected (but unrelaxed) modulus, one can determine a priori the attenuation spectrum—its magnitude and its shape—at least that portion associated with the high-T background under thermodynamic conditions where the shear-inviscid grain boundary assumption holds. Figure 10 shows just this approach: the continuous curves were calculated based on Equation (20) defining τ, with η_{ss} values coming from the creep experiments and E coming from Simmons and Wang (1971); the correlation is remarkable.

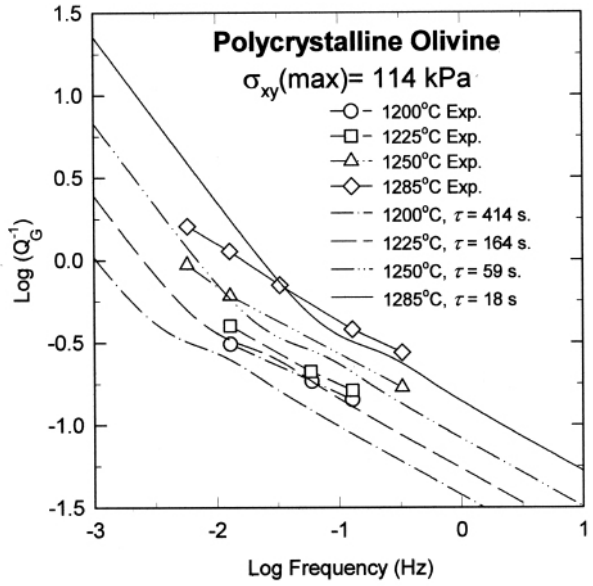

Figure 10. Experimentally measured values of Q_G^{-1} for polycrystalline olivine versus the corresponding predictions of the intrinsic creep transient model. The value of τ for each temperature was calculated via Equation (18) with η_{ss} obtained from the unidirectional creep response of the material and E obtained from Simmons and Wang (1971). The experimental data do not show the transition to the $Q_G^{-1} \propto f^{-1}$ behavior predicted by the model at higher temperatures and lower frequencies; however, the effect of errors inherent in the simplifications of the model are sufficient to explain this inconsistency (cf. Fig. 9). [Used by permission of American Geophysical Union, from Gribb and Cooper (1998) *Journal of Geophysical Research*, Vol. 103, Fig. 10, p. 27275.]

DATA EXTRAPOLATION AND APPLICABILITY OF EXPERIMENTS TO GEOPHYSICAL CONDITIONS

The interpretation of the intrinsic diffusion-creep transient in terms of a grain-boundary-diffusion-limited mechanism was based on a significant database suggestive of such behavior (e.g., Karato et al. 1986; Hirth and Kohlstedt 1995). Nevertheless, the predicted, substantial sensitivity of the dynamics to the grain size in this case (i.e., $\eta_{ss} \propto d^3$ and $\tau \propto d^3$) prompts a direct experimental analysis of the effect, which is required if the experimental data are to be evaluated relative to the geophysical situation of interest (e.g., upper mantle grain sizes, where d is estimated in the range 1 mm to 1 cm (cf. Karato and Spetzler 1990)). The impact of grain size on low-frequency absorption in polycrystalline olivine has recently been measured both in Jackson's laboratory (d in the range 3–24 μm, T in the range 1000–1200°C; Jackson et al. (2002)) as well as in my laboratory (d in the range 4–17 μm, T in the range 1175–1300°C; Bunton (2001); Bunton and Cooper, in preparation). 1200°C experimental data from both studies—the condition where the data sets directly overlap—are shown in Figure 11. Despite the materials being fairly different (Jackson et al. studied aggregates prepared by hot-pressing (i) pulverized San Carlos, Arizona, peridot as well as (ii) powder prepared entirely by sol-gel (solution) processing, while Bunton examined aggregated prepared by vacuum sintering of pulverized Balsam Gap dunite), the agreement of the data, particularly at log f < -1.2, is very strong. The Q_G^{-1} measurements from both laboratories demonstrate that the power-law exponent for the spectra increases (i.e., becomes less negative) as frequency and grain size are increased (and also as temperature is decreased, though confirmation of this point is not available in Fig. 11); for Bunton's data, that slope approaches zero for some conditions. Bunton's creep measurements characterize unequivocally that $\eta_{ss} \propto d^2$, which is a surprise, given the database (already cited) for diffusional creep of olivine. The conventional way to interpret the $\eta_{ss} \propto d^2$ result is to conclude that the steady-state response is rate-limited by lattice diffusion. The activation energy measured for both the creep and attenuation in these experiments, however, is $E_a \approx 650$ kJ mol^{-1}, a value far too high compared to the thermal sensitivities directly measured for lattice diffusion of all component ion species in olivine (e.g., Brady 1995). The "mystery" here most likely involves a threshold phenomenon for diffusional creep that is effected by the distribution of point defects in and near the grain boundaries (Jamnik and Raj 1996); this effect can result in a $\eta_{ss} \propto d^2$ behavior for grain boundary diffusion creep for a very low stress

potential, as employed in these experiments. This argument, though, is beyond the scope of this chapter. Extrapolation of the experimental data with grain size, however, requires use of a $\tau \propto d^2$ relationship, and Equations (18)–(20) can be modified to reflect the behavior.

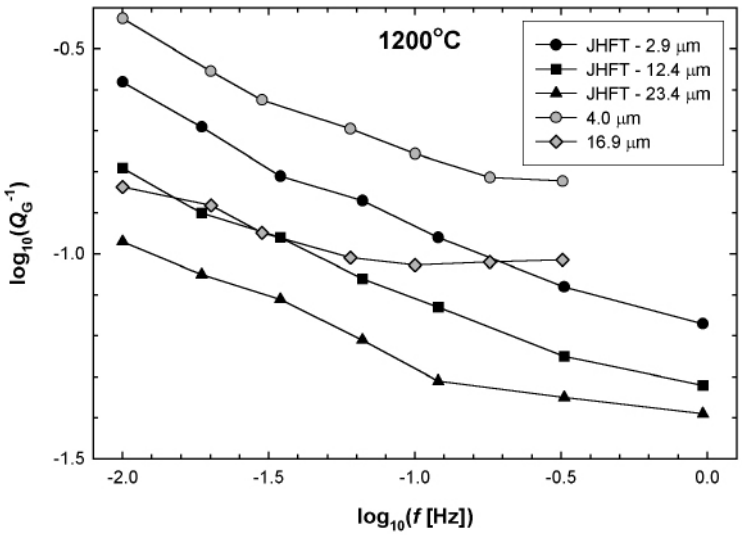

Figure 11. Impact of grain size on the measured attenuation response of polycrystalline olivine: 1200°C data from Jackson et al. (2002) (labeled "JHFT; black solid symbols; high-confining-pressure experiments on aggregates prepared from San Carlos peridot and from chemical sols) and from Bunton (2001) (gray symbols; ambient-pressure experiments on aggregates prepared from Balsam Gap dunite). The grain sizes are as noted in the key. The curves indicate an increase in the value of the power-law exponent *m* (i.e., it becomes less negative) with an increase in frequency.

Figure 12 presents all of Bunton's attenuation data (white circles), extrapolated in frequency based on both temperature (Boltzmann statistics, see Section 4) and grain size (i.e., overall, $\tau \propto d^2 \exp(-E_a/RT)$ with $f \propto \tau^{-1}$, cf. Fig. 9) to conditions of 1200°C and d = 1 mm; one sees clearly that a master curve results for the data, proving the efficacy of the physically based, frequency extrapolation approach outlined above. To this plot has been added (i) the 1200°C attenuation data of Jackson et al. (2002), (ii) the 1200°C attenuation data of Gribb and Cooper (1998), (iii) 1200°C attenuation data for a forsterite single crystal (minimum dimension ~1 mm) that was first plastically deformed to steady state in dislocation creep at T = 1600°C and $(\sigma_1-\sigma_3)$ = 20 MPa and then low-stress attenuation-tested in shear (Gueguen et al. 1989) and (iv) the Andrade model inversion—consistent with the universal attenuation curve—for $\tau \propto d^2$ behavior. The frequency shift of both the Jackson et al. (2002) and Gribb and Cooper data is based on $\tau \propto d^2$ (direct analysis of the Jackson et al. (2002) 1200° data gives $\tau \propto d^{(1.2–2.0)}$, depending on the Q_G^{-1} at which the measurement is made). An oblique view of the graph better reveals the curvature in the model curve. The correlation of the polycrystalline data from different investigations is again revealed as strong. Further, one sees that the extrapolation of the inviscid-boundary model to seismic/teleseismic frequencies for this mantle-like grain size gives Q_G far, far in excess of the values 100–500 cited in many mantle models (e.g., Anderson and Given 1982; Romanowicz and Durek 2000). Besides, it is clear that the polycrystalline data themselves deviate from the model at (the transformed) $f > 10^{-6}$ for this grain size and temperature. It is logical to conclude, then, that a different physical mechanism begins to affect the absorption response with the increase in frequency/drop in temperature/increase in grain size conditions associated with the high-frequency "tail" on the spectrum. The "gentleness" of the deviation from the model suggests that it is the

shear-inviscid grain boundary assumption in the model that is failing, that is, with the change in f, T, d, the serial-kinetic process of grain boundary sliding begins to dissipate, in part, the mechanical energy. This point is the centerpiece of the Jackson et al. (2002) argument concerning their $Q_G^{-1}(d)$ data and its extrapolation in grain size.

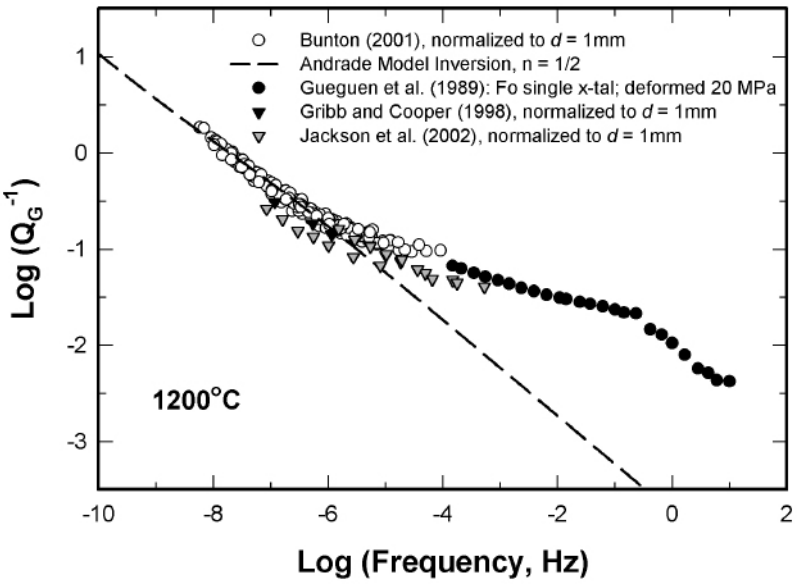

Figure 12. Comparison of a 1200°C, polycrystalline olivine absorption master curve (created from 1200°C data from Jackson et al. 2002, Gribb and Cooper 1998, and all data from Bunton 2001; see text)—for an extrapolation to d = 1 mm—to the 1200°C torsional attenuation response of a forsterite single crystal that was first crept to steady state at 1600°C, 20 MPa (Gueguen et al. 1989). The tail in the master curve, associated with the absorption response(s) of viscid grain boundaries, maps into the response of the deformed single crystal. The correlation suggests low-angle (subgrain) boundaries play a significant—perhaps primary—role in the absorption of the deformed single crystal.

Because it acts in kinetic series with both diffusional and dislocation flow mechanisms—meaning that, under most thermodynamic conditions, it cannot be physically isolated—grain boundary sliding is difficult to characterize. At one extreme, the oft-cited model for grain boundary sliding-effected absorption treats grain boundaries as thin films of a finite width and a constant and finite Newtonian viscosity (Zener 1941). Loading produces sliding displacements on the boundaries, at a rate dependent on their unique viscosity, and elastic loading of triple junctions (hence the description of the physics as "elastically accommodated grain-boundary sliding," e.g., Raj and Ashby 1971). From a mechanics-model perspective, one can imagine a Voigt/Kelvin Solid model placed in mechanical series with a spring (i.e., no plastic response is possible, only anelastic and elastic responses); the resultant model is one form of the "Standard Linear Solid," and its dynamic response is an exponential-decay-based Debye peak. τ_C in this case is given by (Nowick and Berry 1972, p. 437):

$$\tau_C = \eta_b d / \xi G , \tag{21}$$

where η_b is the boundary shear viscosity and G is the unrelaxed material shear modulus. The grain-size scaling for the peak location goes as $\tau_C \propto d$, in that strain is characterized as the relative displacement across the boundary normalized by the grain size. An important ramification of the model is that the magnitude of the absorption is independent of grain size: a change in d solely causes a shift in frequency of the Debye peak with no change in its height.

A nice example of the phenomenon is the absorption response of hot-pressed, polycrystalline Si_3N_4 ceramics (e.g., Mosher et al. 1976; Pezzotti et al. 1996). Si_3N_4 is one of the few materials where it is apparently all-but-impossible to form crystalline grain boundaries: in these materials, all grain boundaries have been replaced by ~1-nm thick films of amorphous silica or silicate (e.g., Clarke 1987). The chemistry (and thus the molecular structure and, with it, the viscosity) of these films is controlled by oxide additives. In general, the Newtonian viscosity of these thin films is $>10^3$–10^4 times smaller than that expected of diffusional processes in the Si_3N_4 proper. It is this extreme viscosity difference that allows experimental "access" to the boundary-sliding relaxation: to first order, the conditions envisioned by Zener (1941) (i.e., pure elastic accommodation of boundary sliding and little other time-dependent response) are met, quite clean Debye peaks are characterized and, from them, η_b and its temperature sensitivity are determined.

The Debye-peak grain-boundary absorption response matching the Zener (1941) model has been seen only rarely in metals. Kê's (1947) work on high-purity aluminum is the classical example: the study revealed the single Debye peak whose magnitude correctly matched theoretical prediction and as well as the property of being independent of grain size; in addition, the $\tau_C \propto d$ was confirmed. Other careful studies comparing polycrystalline metals with single crystals (reviewed in Nowick and Berry (1972) and Lakes (1999)) periodically reveal a broad absorption peak of low magnitude in the polycrystalline material, one barely "competing" to be seen over the power-law background absorption. The interpretation of such a response is problematic. The simplest (albeit not unique) defensible interpretation is that the constant-boundary-viscosity assumption of the Zener (1941) model is, in general, inappropriate: actual grain boundary sliding (that is, in materials with crystalline grain boundaries, in contrast to the Si_3N_4 example cited earlier) involves chemical diffusion and the glide+climb motion of primary and secondary grain boundary dislocations (cf. Ashby 1972). In that grain boundary structure is a strong function of, for example, the relative orientation of grains, the loss of degeneracy of η_b is easily contemplated.

Of course, not even a broad grain-boundary-sliding peak is evident in the polycrystalline olivine data presented in Figures 11 and 12. This is perhaps not surprising: when the selection of thermodynamic and microstructural conditions is such that two (or more) serial-kinetic processes are vying for rate control, the impact on the measured kinetics is often subtle. Crossman and Ashby (1975) have modeled the plasticity behavior of polycrystals, specifically to gage the impact of the grain boundary response on the kinetics. The impact on bulk deformation kinetics of changes in thermodynamic conditions that cause the boundaries to evolve from inviscid to (uniformly) Newtonian-viscous to rigid is demonstrated to be very minor: at constant T, the effect is a ~10% increase in the stress providing a given strain rate, with the stress transition being played out over less than a half-order of magnitude in strain rate. Not minor, however, is the spatial distribution of strain (and thus of energy dissipation) within individual grains corresponding to the transition: for an overall Newtonian-viscous aggregate, the strain associated with viscous grain boundary sliding evolves from 15% of the total to 0%, but played out over two-to-three orders of magnitude in strain rate. Because of this serial-kinetic coupling of the diffusional based transient flow with the viscous response(s) of grain boundaries, simple application of superposition, e.g., as is done with parallel kinetic processes, is not physically sound.

What can be said, then, of extrapolation of experimental data on grain-boundary effects in attenuation to the geological setting? For polycrystalline olivine, Jackson et al. (2002) have noted the complexities of physical behavior associated with the inviscid-to-

viscous transformation of the grain boundaries, including the ineffectiveness of a straightforward application of superposition of the effects represented here by Equations (18) and (21), and so chose to apply the essentially empirical Schoeck et al. (1964) equation to their data, modified to include the apparent effect of grain size, i.e.,

$$Q^{-1} \propto [f^{-1} d^{-1} \exp(-E_a / RT)]^{\alpha}. \tag{22}$$

Their best-fit lines to those log Q^{-1} vs. log f data at higher-frequency and lower temperature give a value for α of 0.27 and a value of E_a ~400 kJ mol^{-1}. Jackson et al. (2002) continue by showing that a "vertical" translation (i.e., a shift in Q^{-1} with changes in grain size and/or temperature) of their data to grain sizes thought appropriate for the upper mantle produce $Q^{-1}(f)$ results in rational agreement with values measured seismologically. Jackson et al. (2002) conclude, accordingly, that the "same grain-size-sensitive processes [active in the experiments] might be responsible for much of the observed seismic-wave attenuation." Barring a better understanding of the physics of absorption of extended defects, like grain and phase boundaries, both Jackson et al.'s approach to data analysis and their conclusions must be considered reasonable.

Discerning the physics of absorption processes of extended defects, and thus how absorption is affected by microstructure, is the present "cutting edge" of experimental research in attenuation/internal friction. Of interest in both geophysics and materials science is the specific impact of deformation-induced microstructure on the absorption behavior. Figure 12, thus, presents the provocative comparison of the polycrystalline olivine data with that for the attenuation response of a deformed forsterite single-crystal (Gueguen et al. 1989). In these experiments, the single crystal was first deformed to steady state at 1600°C and 20 MPa differential stress and, subsequently, a slice with minimum dimension 1 mm was tested in reciprocating shear at 1200°C. One sees clearly that the tail of the polycrystalline master curve "maps" into the single-crystal data. Further, there exists no high-angle grain boundaries to effect absorption (crystals not "pre-deformed" demonstrated a high-temperature experimental $Q_G^{-1} \sim 10^{-2}$ that was essentially frequency independent). The result suggests strongly that low-angle (subgrain) boundaries in the single crystal, a result of the 20-MPa plastic deformation, are of primary importance in the overall attenuation response, that is, if the scale of these low-angle boundaries matches reasonably the 17–24 μm associated with the "tail" of the polycrystalline data. Such is the case: in a high-T, steady-state dislocation rheology, the single crystal must develop a polygonized microstructure, that is, there is developed a three-dimensional network of low-angle subgrain boundaries whose mean spacing (and spacing distribution) is set by the level of differential stress (and little-effected by T) (cf. Glover and Sellars 1973; Twiss 1977; Kohlstedt and Weathers 1980; Stone 1991). For forsterite at 1200°C, a 20 MPa differential stress creates a mean subgrain boundary spacing of ~20 μm.

The physical implication, then, is that a small-amplitude, oscillatory variation in stress, one that is added to a nominally constant, and significantly greater differential stress that is effecting dislocation creep in a material, is "sampling" the deformation-induced microstructure, and particularly the network of subgrains. Such a perspective on the high-temperature background absorption behavior and its interrelation with the subgrain network is consistent fully with models attempting to formulate a microstructural foundation for the phenomenological mechanical (plasticity) equation of state. The equation-of-state approach (theory: e.g., Hart (1970); experiments in ionic solids: e.g., Lerner et al. (1979); Covey-Crump (1994)) suggests that a *single*, internal state-variable can be used to describe the strain-effected "hardness" (i.e., the microstructural resistance to flow) of a material. The model of Stone (1991) correlates this state variable to the statistical distribution of low-angle boundaries and how this

distribution is affected by changes in stress and by accumulated strain: the steady-state distribution is primarily dependent on the applied stress, while the evolution of the distribution—effected by diffusion-based processes within the low-angle boundaries—is strain sensitive. Recent experiments on the flow of halite (Plookphol 2001), comparing/correlating the deformation kinetics and deformation-induced microstructures from both creep experiments and load-relaxation experiments, confirm many of Stone's hypotheses. While this research correlating deformation-induced microstructure and "hardness" is young, one ramification is clear: with experimental care, the relative absorption effects of high-angle and low-angle boundaries (as well as of solid-state phase boundaries) can be deconvolved, physical models for these phenomena formulated and tested, and the results extrapolated. The possibilities of a more exacting and robust way of interpreting seismic Q^{-1} data, i.e., its use as a prospecting tool to understand structures and stresses (and perhaps strains) in active tectonic terranes, seems within the realm of reason.

SUBGRAIN ABSORPTION AND THE ATTENUATION BAND

As evidence of the possibilities, consider the room-temperature attenuation spectra ($\tan \delta \equiv Q_G^{-1}$), presented in Figure 13a, for various phases in the solder system indium-tin. These data are from Lakes' laboratory, collected on his "broadband viscoelastic spectrometer" (Brodt et al. 1995); the breadth of frequencies explored is extraordinary. The data for γ-$InSn_4$ (solid squares) and β-γ eutectic (solid triangles) data were published earlier (Lakes and Quackenbush 1996); the data for single-phase β-In_3Sn ("×" symbol; between 10^{-1} and 10^3 Hz, these data are so dense that they appear as a solid line) represent a recently inaugurated collaboration with Lakes (McMillan et al., submitted). β-In_3Sn is not an intermetallic compound but rather is an endothermic solid solution having the same body-centered tetragonal (BCT) crystal structure as pure In; as a consequence, β-In_3Sn has a limited number of dislocation slip systems and the Peierls barriers to slip are high. Similarly, γ-$InSn_4$ is also an endothermic solid solution with a hexagonal crystal structure, again having limited slip systems and a high Peierls barrier. β-γ eutectic is, thus, a two-phase (with different crystal structures) solid; in this case, γ grains are dispersed within a continuous, polycrystalline β phase. At frequencies in the range 10^{-3} to 1 Hz, one sees that the eutectic is significantly more absorbing than is either component phase individually: clearly, one cannot apply a simple rule-of-mixtures to model the data for these frequencies. Solid-state β–γ phase boundaries are perhaps so demonstrated to be more potent mechanical absorbers than β grain boundaries or subgrain boundaries in this frequency range; affirmation of this postulate requires a better understanding of absorption in the individual phases that constitute the eutectic.

To better probe the physics of the broadband power-law absorption behavior, we have initiated a hierarchal study with single-phase β, using deformation and thermal processing to vary the dislocation (sub)microstructure. The baseline behavior—the as-cast condition (labeled "tan δ; cast β In-Sn")—is that presented in Figure 13a. The data display an attenuation plateau, $m \sim 0$, in the region 10^{-1}–10 Hz. Beyond 10 Hz, the data trend back towards the $m \sim 0.3$ slope characteristic of the frequencies below 10^{-1} Hz; as such, a description of the data above 10^{-1} Hz as a "broad hump" is perhaps appropriate. (Note, too, absorption behavior of single-phase γ has a similar plateau for frequencies ≥10 Hz. The "tail" visible in the polycrystalline olivine data presented in Fig. 12 is also consistent with this spectral feature.)

Figure 13b presents results of a parametric study in which the torsional absorption spectra (emphasizing the frequency range 10^{-1}–10^3 Hz) of β specimens were measured as functions of various specimen preparations. These preparations were serial and cumulative, meaning that specimens were mechanically tested after each step of process-

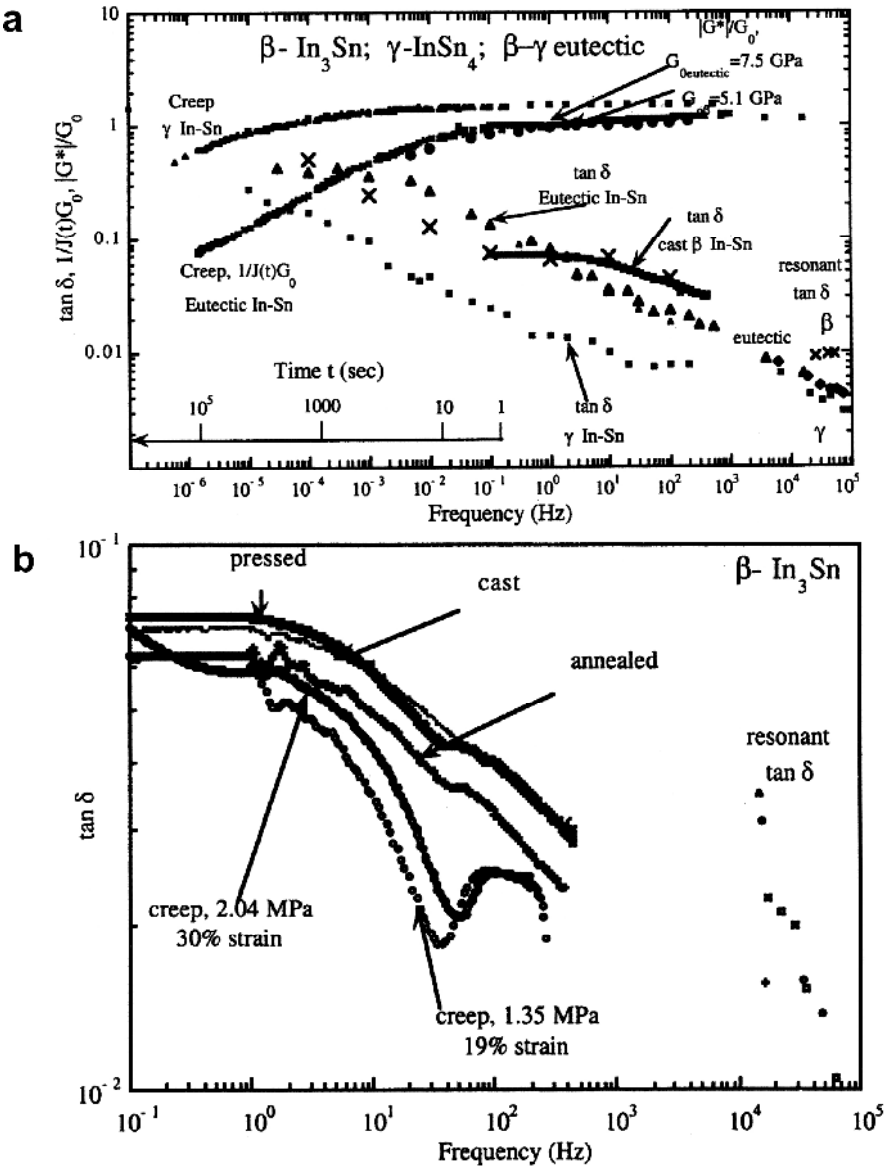

Figure 13. (a) Torsional tan δ ($\equiv Q_G^{-1}$) and normalized complex shear modulus (|G*|) as functions of frequency, and creep compliance (J(t)) as a function of time, for β-In_3Sn (×), γ-$InSn_4$ (■) and the β–γ eutectic (solid triangles), all in the as-cast condition and at room temperature. (The tanδ data for β-In_3Sn in the frequency range 10^{-1}–10^3 Hz is so dense as to appear as a solid line.) One sees that the power-law absorption behavior holds for both single-phase β and γ materials at low frequency ($m \approx 0.3$); both β and γ deviate from this behavior at increasing frequency (~10^{-1} Hz for β; ~1 Hz for γ). (b) Effect of processing conditions on the tanδ of single-phase β-In_3Sn specimens. The processing followed a hierarchy of as-cast ("cast" in the figure); cast + pressed (high-rate, high-strain deformation; "pressed"); cast + pressed + annealed ("annealed"); cast + pressed + annealed + creep ("creep," with the stress and strain noted). One sees a significant effect of the creep treatment: despite an increase in lattice dislocation density due to the tensile creep deformation, tan δ actually decreases. In addition, an absorption peak is created at ~10^2 Hz. Both results suggest an important perhaps dominant—role of low-angle boundaries in effecting the power-law absorption.

ing. Beyond the as-cast condition (spectrum marked "cast" in Fig. 13b, which is a replication of a portion of the spectrum shown in Fig. 13a), specimens were (i) plastically deformed at a high rate to greater than 60% compressive strain at 293 K (producing the absorption spectrum marked "pressed"), followed by (ii) annealing at 390 K (~95% of the

melting temperature) for several hours (producing the spectrum marked "annealed"), followed by (iii) high-strain, plastic deformation in tension by dislocation creep (cf. Frost and Ashby 1982). Two different creep stresses were studied, 1.35 and 2.04 MPa. The absorption spectra are marked "creep;" the respective deformation stress and strain are noted as well. Optical microscopy of the specimens subsequent to various treatments revealed little effect of processing on grain shape or size: β grains remained nominally equiaxed with mean grain sizes ranging from ~500 μm for the "pressed" specimens to ~700 μm for the "annealed" specimens and, despite the large accumulated strain, creep subsequent to annealing had no statistically significant affect on the size or shape of the grains. In that torsional-specimen cross-sections were approximately 3×3 mm, the number of grains making up that cross-section was small. Torsional maximum strains in the absorption experiments were 10^{-6}; despite the presence of lattice dislocations in the "pressed" and "creep" specimens, the materials were proven linearly viscoelastic at this strain.

One sees clearly in the data (Fig. 13b) that, despite the creep deformation that must endow the specimens with a significantly higher density of mobile lattice dislocations than are remnant in an "annealed" specimen, the absorption of the crept specimens is significantly *lower*. Specifically, the spectra demonstrate a diminishment of the plateau/broad hump and demonstrate, too, the sharpening of a Debye peak near $f = 10^2$ Hz. Because of the limited slip systems in the BCT-structure β, the tensile creep must result in a significantly limited distribution of subgrain boundary structures—a distribution in dynamic equilibrium with the applied tensile stress. The spectral peak at 10^2 Hz results from the absorption of a specific boundary structure (cf. Yan and Kê 1987), one obviously now more prevalent due to strain accumulation. Further, one sees that, for the "creep" specimens, absorption is apparently increased—actually, it is shifted to higher frequency—by deforming at a higher creep stress. The amount of this frequency shift is exactly that predicted by the change in τ (Eqn. 18), when d is considered to be the mean subgrain size, the magnitude of which is calculated from the mean-subgrain-size/differential-stress semi-empirical "calibration" of Twiss (1977) (and employing the measured, high-frequency shear modulus).

An obvious question to ask, then, is whether the shallow peak near $f = 10^{-1}$ Hz in the absorption data for the deformed forsterite single crystal (Fig. 12) is related to a similar concentration of specific low-angle boundary structures. Gueguen et al. (1989) did not comment on this aspect of their data. Nevertheless, with limited slip systems, olivine, too, realizes a limitation on the structures of low-angle boundaries (e.g., Ricoult and Kohlstedt 1983; Bai and Kohlstedt 1992a).

Finally, the diminishment of absorption with the addition of lattice dislocations to the material (Fig. 13b) should give pause to any generalized, qualitative speculation that "dislocation mechanisms" (i.e., the behavior of "free" lattice dislocations as opposed to the dislocation arrays constituting low-angle boundaries) are dominating a power-law, high-temperature-background absorption response. Inevitably, dislocation "vibration" with cyclic loading occurs, and must lead to nonlinearities in absorption (e.g., Lakes 1999, Ch.8). Yet under the thermodynamic (high temperature, low deviatoric stress), microstructural (polyphase, mineral (ionic) aggregates with each phase having a high Peierls barriers to dislocation glide) and frequency conditions of interest in geological settings, such mechanisms of absorption may prove of little consequence.

IMPACT OF PARTIAL MELTING

The impact of partial melting on low-frequency mechanical absorption depends primarily on (i) the spatial distribution of the melt and crystalline phases, (ii) the relative

volume fractions of these phases and (iii) the practical rheological contrast of these phases. Early geophysical analyses to correlate materials properties with their capability to absorb shear waves concentrated on the spatial distribution of a liquid phase at the scale of the grain size of the crystalline residuum (e.g., Walsh 1969; Birch 1970; Mavko 1980). For example, it is easy to comprehend that a partial-melt microstructure in which all solid-state grain and phase boundaries are replaced by a homogeneous, low-viscosity liquid will be far more absorbing of shear waves (at a fixed frequency related to the viscosity of the liquid films—cf. the Si_3N_4 example cited earlier) than a system where grain and phase boundaries remain melt-free. Waff (e.g., Waff and Bulau 1979; Waff 1980; Waff and Faul 1992) inaugurated the petrologic study of partial-melt morphology, which followed in philosophy the microstructure topology work of Smith (1952). Waff defined "textural equilibrium" as the minimization of solid-solid (grain boundary or solid-state phase boundary) and solid-liquid interfacial energy; in olivine-basalt partial melts, under hydrostatic conditions and for a small volumetric melt fraction, textural equilibrium sees the liquid phase confined to three-grain ("triple") junctions and four-grain corners, forming a 3-D interconnected melt network, with melt-free olivine grain boundaries. That the grain boundaries in these materials were indeed melt free was confirmed to a resolution of 0.5 nm using high-resolution transmission electron microscopy (HRTEM; e.g., Vaughan et al. 1982; Cooper and Kohlstedt 1982), a result confirmed by high-resolution transmission analytical electron microscopy (HRAEM; Kohlstedt 1990). The result remains controversial: for example, de Kloe et al. (2000) argue from HRTEM/AEM evidence that a deviatoric stress (≥100 MPa) changes this textural equilibrium so as to produce nm-scale melt films that replace grain boundaries. The chapter in this volume by David Kohlstedt, examining the rheology of partial melts and the physics of melt segregation, presents the breadth of microstructural evidence and associated arguments. Nevertheless, in drained mafic-to-ultramafic material at low melt fraction, the vast majority of the liquid phase is confined to triple junctions and four-grain corners.

The impact of grain-scale, partial-melt textural equilibrium on attenuation, then, involves three possible effects that are perhaps distinguishable experimentally: (i) long-range (i.e., beyond the grain scale) melt migration based on gradients in hydrostatic pressure (a bulk-modulus-mode absorption); (ii) melt "squirt" (Mavko and Nur 1975), a shear effect that adjusts the volume of adjacent triple junctions at the grain scale; and (iii) any shear effect that might arise from melt films replacing grain boundaries and/or solid-state phase boundaries.

Long-range melt migration is best contemplated following a D'Arcy flow model in which the compaction of the crystalline residuum imparts momentum to the interconnected liquid phase; in the geophysics literature, the seminal papers of McKenzie (1984), Richter and McKenzie (1984) and Scott and Stevenson (1986) present these ideas, now known as "compaction theory." The relative velocities of the crystalline residuum and the liquid are linearly proportional to the inverse gradient of the pore fluid pressure, with the constant of proportionality being the permeability of the residuum, i.e.,

$$\boldsymbol{u} - \boldsymbol{U} = -\left[k(\phi, d) / \eta_f \right] \nabla \boldsymbol{\Pi} , \tag{23}$$

where

$$\nabla \boldsymbol{\Pi} = \eta \nabla^2 \boldsymbol{U} + \left(\zeta + \eta/3\right) \nabla \left(\nabla \cdot \boldsymbol{U}\right) - \left(1 - \phi\right) g \Delta\rho - H\left(\gamma_{sl}, \phi\right) \nabla \phi . \tag{24}$$

In Equation (23), $\boldsymbol{u}$ and $\boldsymbol{U}$ are the velocities of the melt and crystalline residuum, respectively, k is the permeability (which is a function of the volumetric melt fraction, ϕ, and the grain size), η_f is the shear viscosity of the liquid and $\nabla \boldsymbol{\Pi}$ is the gradient in pore

fluid pressure; in Equation (24), η is the shear viscosity and ζ the bulk viscosity of the partial-melt aggregate, respectively, g is the acceleration of gravity, $\Delta\rho$ is the density difference between liquid and crystalline phases and γ_{sl} is the interfacial energy ("surface tension") of the crystal (solid)-liquid interface. The first two terms in Equation (24) represent pressure gradients affected by shear and dilatational deformation, respectively, the third term is the buoyancy effect and the last term (Stevenson 1986; Cooper 1990) is the restraining effect of capillarity. In the geophysical context, gravity drives the liquid phase upwards while the residuum compacts downward; capillarity restrains the expulsion of all of the melt. From a chemical kinetics perspective, buoyancy-driven melt migration is obviously a serial-kinetic process based on a geometrical constraint: liquid is not expelled unless the residuum compacts. Parametric analysis of the equations reveals a characteristic "compaction length," δ_c:

$$\delta_c = [k(\zeta + 4\eta/3)/\eta_f]^{1/2} \ ; \tag{25}$$

δ_c is the instantaneous length over which the compaction is rate limited solely by the capabilities of the residuum to deform (i.e., the actual flow of the liquid phase dissipates none of the energy in compaction). Beyond δ_c, energy dissipation is convolved between the deformation of the residuum and shear flow of the viscous liquid, although at scales large compared to δ_c, the shear flow of the liquid should be rate-limiting.

Bulk-modulus anelasticity for a partial melt arises due to the restorative force of capillarity: a hydrostatic compressional force promotes compaction; capillarity (the Laplace-Young relationship, e.g., that defines the correlation of the pressure in a bubble to its surface tension) promotes swelling upon removal of the applied force. Flexural creep experiments, which optimize the melt-migration driving force while minimizing the driving force for shear creep of the aggregate, combined with both microstructural analyses and strain-relaxation measurements, proved the operation of the long-distance migration mechanism and its anelastic nature (Cooper 1990; Gribb et al. 1994). The seismic-frequency absorption response for this mechanism was measured directly for partially molten, Newtonian-viscous silicate partial melts in reciprocating flexure ((ortho)enstatite glass-ceramic, Gribb and Cooper (1995)) and reciprocating compression (Co-Mg olivine-"basalt", Gribb et al. (1994)). In both these cases of Young's-modulus-mode loading, the effective δ_c was significantly smaller than the specimen size: flow of the liquid phase rate-limited the anelastic response. The absorption spectra revealed the power-law behavior, with a very-low $m \sim 0.10$–0.14 (see Fig. 6 for the glass-ceramic data). As noted earlier, a single, non-exponential-decay mechanism related to the D'Arcy-flow (diffusion)-effected migration of the flexural-specimen's neutral axis (or to the growth of the compaction layer—from the specimen's free sides to the specimen center—in compression specimens) accurately models the absorption response for this long-range melt migration.

Given the thermodynamics of capillary forces, the long-distance-migration mechanism is not expected to be operative in pure-shear loading. As a consequence, shear experiments can isolate the other two, grain-scale partial-melt absorption effects listed above. Gribb and Cooper (2000) compared the shear absorption responses of fine-grained ($d \sim 3$ μm) olivine aggregates with and without the addition of 5 wt % (6 vol %, i.e., $\phi \sim 0.06$) of a texturally equilibrated, K^+-doped basanite melt (the melt composition was selected to be saturated with respect to olivine as well as to have a low-enough viscosity to provide a δ_c that was significantly greater than the specimen size). Experiments were done in the regime of (f,d,T) characteristic of the shear-inviscid boundary assumption being applicable to the melt-free specimens. The 1250°C result, characteristic of all the experiments, is presented in Figure 14a: the partial melt specimens showed essentially the same power-law absorption spectra as do the melt-free

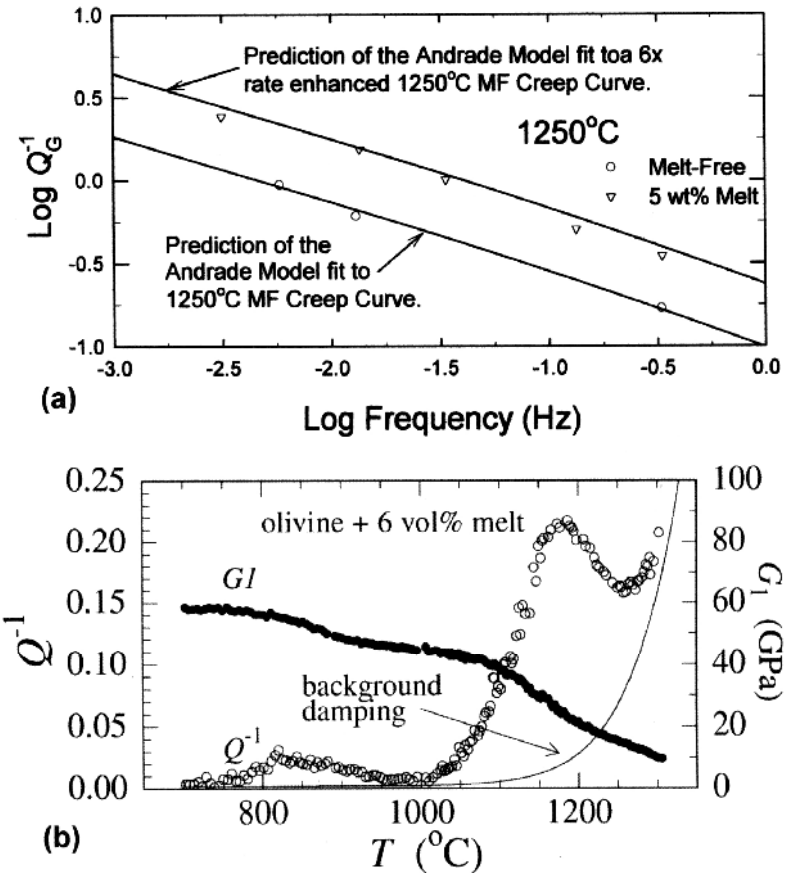

Figure 14. Effects of grain scale partial melting—at low melt fraction and the textural equilibrium corresponding to nominally hydrostatic pressure (melt-free grain boundaries)—on the shear attenuation response of olivine. (a) Sub-resonant behavior. At the high-temperature and/or low-frequency conditions where the inviscid grain boundary assumption holds, partial melting affects the absorption spectrum solely by its shifting to slightly higher frequency. The magnitude of the frequency shift is predicted by the effect of partial melting on the aggregate η_{ss}, following the model of Cooper et al. (1989). There is no apparent disaggregation of the material—with consequent dramatic drop of shear modulus—because of the presence of melt. [Used by permission of American Geophysical Union, from Gribb and Cooper (2000), *Geophysical Research Letters*, Vol. 27, Fig. 3, p. 2343.] (b) Resonant behavior at f ~2 Hz. Two Debye peaks are revealed: the one at high temperature may be related to the grain-scale "melt squirt" phenomenon envisioned by Mavko and Nur (1975); alternatively, it may represent a solid-state grain-boundary absorption. [Used by permission of Columbia University Press, from Xu et al. (2002). In *MARGINS Theoretical and Experimental Earth Science*, edited by G. Karner, Fig. 10.3, in press.]

specimens ($Q_G^{-1} \propto f^{-0.4}$), with the partial melt spectra shifted to a higher frequency that corresponds to an decrease in η_{ss} of a modest factor of 6. In the figure, a shift of the Andrade-Model inversion for the melt-free material, corresponding to this decrease in η_{ss} for the partial melt, predicts beautifully the partial melt attenuation. The important interpretation is that relative to point (iii) above: there is no melt-effected plummeting of viscosity or shear modulus, nor a dramatic increase in shear attenuation, as might be anticipated if all grain boundaries were replaced by films of a low-viscosity liquid. Further, the thermal sensitivity (activation energy) of both creep and attenuation responses were identical between partial-melt and melt-free materials, clearly suggesting that the same physical process rate-limits both creep and attenuation in both materials.

The results (i.e., the magnitude of decrease in η_{ss} and the consequent effect on the attenuation spectra) are consistent fully with the model for melt-enhanced diffusional creep in which diffusion through grain boundaries is rate limiting and the triple-junction melt network, representative of textural equilibrium, provides a partial short-circuit for diffusion (Cooper et al. 1989; see the chapter in this volume by Kohlstedt).

Shear resonance (torsion pendulum) experiments (Xu et al. 2002) performed on fine-grained ($d \sim 20$ μm) olivine-basalt aggregates ($1 \le f$[Hz] ≤ 10; $22 \le T$[°C] ≤ 1350; $0.004 \le \phi \le 0.13$) reveal two distinct Debye peaks, one centered on $T \approx 875$°C and the other on $T \approx 1175$°C (the data for $\phi = 0.06$ is presented in Fig. 14b). The high-T peak has a magnitude that is weakly sensitive to ϕ: $Q_G^{-1} \sim 0.3$ for $\phi = 0.13$; $Q_G^{-1} \sim 0.1$ for $\phi = 0.004$. The low-temperature peak is associated with the glass transition of the quenched basalt; the high-temperature peak, however, speaks either of a melt-squirt effect and/or of a grain-boundary effect in shear absorption. Melt squirt is defined as an exponential-decay absorption mechanism with a characteristic time, τ_{ms}, given by (cf. Mavko 1980):

$$\eta_f = (\tau_{ms} K_f / 40)(R/d)^2, \tag{26}$$

where K_f is the bulk modulus of the liquid and R is a measure of the cross-section of the triple-junction "tube." Xu et al. (2002) calculate that, for the characteristic τ_C of their experiments, the η_f is too high, by an order of magnitude, than that of a bulk, olivine-saturated liquid basalt; as a consequence, they interpret the high-temperature peak to be one associated with the Zener grain-boundary absorption (i.e., Eqn. 21). Their argument continues by demonstrating that an extrapolation of their data to $\phi = 0$ matches well the "plateau" result of Bunton (2001) for melt-free olivine of similar grain size. It seems premature, however, to completely rule out a melt-squirt contribution in this absorption peak. For example, the viscosity of a bulk liquid may not accurately reflect the shear resistance of a silicate melt within a ≤1 μm "diameter" triple junction tube, particularly considering that the melt flow involves, too, stress-effected chemical reaction with the tube (cf. Riley and Kohlstedt 1991). Further, the significant difference in the thermal sensitivity for their background absorption ($E_a \sim 600$–650 kJ mol^{-1}, which is related to grain boundary diffusion and, most likely, to grain boundary viscosity as well) compared to that for the measured τ_C of the Debye peak ($E_a \sim 300$–350 kJ mol^{-1}) suggests a distinctly different physical process controlling the latter phenomenon. A melt-induced dissipation peak superposed on the power-law absorption response of melt-free olivine has also been observed recently in sub-resonant torsion experiments by Jackson et al. (2001).

A critical factor not yet addressed in any attenuation experiments on partial melts is the role played in absorption by incipient melt segregation beyond the grain scale. Geochemical evidence strongly indicates that melt flow at the grain scale must be very limited in extent, that is, upon formation of melt it must be focused into larger channels so as to avoid continuous reaction with the crystalline residuum (e.g., Spiegelman and Kenyon 1992). Arguments based on the thermodynamics of irreversible processes suggests that a fractal drainage system should prove effective to this end (e.g., Hart 1993). Consistent with the fractal hypothesis, the incipient process of beyond-grain-scale phase separation of melt and crystalline residuum, driven by deformation and affected in scale by the relative values of (bulk-specimen) strain rate and δ_c, has recently been demonstrated experimentally (Holtzman et al. 2001). Correlation of this scaling with the seismic-frequency absorption response for the material overall is an experimental challenge with obvious important implications.

IMPACTS OF DEFECT CHEMISTRY (INCLUDING WATER) AND THE STRUCTURE(S) OF INTERFACES

The rates of chemical diffusion and of temperature-dependent rheology of crystalline solids depend directly on the concentrations of point defects on the crystal lattice. These point defects include vacancies (missing ions or atoms), interstitials (ions/atoms placed in the structure in interstices not occupied in the "perfect" crystal structure) and substitutionals (e.g., as occurs in a solid solution); they additionally include bonded complexes of these single defects as well as the jogs and kinks on lattice dislocations. Made thermodynamically stable by the configurational entropy of their distribution on the lattice, the concentrations of point defects are set by the temperature, pressure (in the limit, they can perhaps be set solely by temperature and pressure—these are the *intrinsic* point defects), deviatoric stress, and by the various chemical potentials defining chemical equilibrium in the system. Indeed, the concentrations of point defects are the physical manifestation of chemical activities within a crystal. In minerals—because the bonding is primarily ionic and, thus, the energy gap between the valence and conduction bands is so large—point defects carry a charge; as such, equilibrium requires that the product of concentration and valence of the positively charged defects equals that of the negatively charged defects; this condition is part of the overall charge neutrality requirement for the crystal. The large band gap also insures that, in the geologic setting, point defect concentrations are affected significantly by changes in the activities (fugacities) defining the equilibrium; this situation is defined as the *extrinsic* condition. In that most minerals contain transition-metal cations, even in very small concentrations, additional important point defects include conduction electrons and electron holes, which are (for example) transition-metal cations having either a too-small valence or a too-large valence, respectively, relative to that valence required for neutrality on the cation site of interest. The concentrations of conduction electrons and electron holes, and therefore (because of the charge-neutrality constraint) the concentrations of most of the other point defects on the lattice, are consequently affected significantly by the oxygen fugacity. (The best pedagogical treatise on point-defect thermodynamics in ionic materials and its application to dynamic processes is the text by Schmalzried (1995).)

The effect of point defect concentrations on mechanical absorption is fourfold (cf. Karato 1995): (i) the defects can perhaps affect the bond strength in the material, and so affect the modulus; (ii) at very high concentrations, the defects can bond and this polar "complex" can respond to stress in a similar manner to that producing the Snoek relaxation described earlier; (iii) the defects affect the rates of all dynamic processes including chemical diffusion and the climb and glide of lattice dislocations and of primary and secondary grain boundary (phase boundary) dislocations; and (iv) the defects affect the structure of grain boundaries and of solid-state phase boundaries, which, in ionic solids, also includes an electrostatic space charge penetrating into the grains on either side of the boundary. Because, in general (though not including substitutional solid solutions of widely ranging concentration), the total concentration of point defects is usually very small, effect (i) can be considered of little consequence. Similarly, the formation of defect complexes is prevalent at lower temperatures and the frequencies anticipated for their mechanical absorption are far higher than those of interest seismologically; effect (ii) can also be set aside. Effects (iii) and (iv), however, are significant to this discussion.

The dynamic effect of point defect concentration (point (iii) above) is often probed by measuring the impact of various chemical fugacities on, for example, viscosity (or, in non-linear systems, effective viscosity). What is discovered experimentally (and supported by point-defect thermodynamics theory) is a power-law dependence, that is,

viscosity is characterized as:

$$\eta \propto f_{\mathrm{ox1}}^{a} f_{\mathrm{ox2}}^{b} \cdots f_{\mathrm{O_2}}^{c} \exp(E_{\mathrm{a}} / \mathrm{R}T), \tag{27}$$

where f_j is fugacity of species j (ox1 and ox2, etc., representing different crystalline oxides that are components of the phase(s) whose viscosity is being probed). The values of power-law exponents a, b, and c (± the value of E_{a}) determined in experiments are compared to theoretical models to discern the specific point defects affecting/effecting the physical behavior. The careful work of Bai et al. (1991) probing the impacts of oxygen fugacity and orthopyroxene (or magnesiowüstite) activity on the dislocation creep rate of single-crystal olivine is a fine example of the application of point defect thermodynamics to mechanical response.

It has long been known that water fugacity ($f_{\mathrm{H_2O}}$) has a dramatic effect on the viscosity of silicates (both crystalline and amorphous), decreasing it dramatically. Griggs (1967) described the phenomenon as "hydrolytic weakening;" the experimental rock physics community has been exploring the phenomenology of this chemical/mechanical effect ever since (the chapters by Jan Tullis and by Greg Hirth in this volume detail the current understanding). The phenomenology suggests clearly that hydrolytic weakening is best contemplated from the perspective of (extrinsic) point defect thermodynamics (i.e., relationships similar in form to Equation (27) can be defined for $f_{\mathrm{H_2O}}$-affected viscosity; e.g., Hobbs (1981)). Identifying the specific point defect(s) responsible for hydrolytic weakening (which could vary for different silicate phases) remains difficult and controversial; the experimental work of Kohlstedt and co-workers, for example, on the reaction of water with various polymorphs of $(\mathrm{Mg,Fe})_2\mathrm{SiO_4}$ illustrates well the confluence of experiment with point-defect theory (e.g., Mackwell and Kohlstedt 1990; Bai and Kohlstedt 1992b; Kohlstedt et al. 1996). These studies additionally suggest that the primary source of water in the mantle is not that incorporated in the ("perfect") structure of hydrous minerals, but rather as extrinsic point defects in the "anhydrous" minerals.

To zero-th order, then, the impact of chemical environment (via its effect on point-defect concentrations—including water-related extrinsic defects) on attenuation is straightforward: impacts on viscosity cause changes in the various τ_{C}'s with consequent frequency shifts in the Q^{-1} spectra. For example, in that recent grain boundary diffusion creep studies on polycrystalline olivine demonstrate that $\eta_{\mathrm{ss}} \propto f_{\mathrm{H_2O}}{}^{-1}$ (Mei and Kohlstedt 2000; cf. Karato et al. 1986), the effect on the absorption model presented in Equations (18) and (20) (Fig. 9) is easily calculated.

There are, however, more profound issues that, while not yet explored directly experimentally, bear contemplation with regard to the impact of point defects, and particularly water-related defects, on the mechanical absorption of mantle material. In partial melting, for example, partitioning of water between the crystalline residuum and the silicate melt functions both to increase the solid-state viscosity of the olivine and lower that of the melt; calculations of the partitioning, integrated with the understanding of its effects on rheology (Karato 1986; Hirth and Kohlstedt 1996), affect the understanding of upper-mantle dynamics, particularly melt segregation. As for attenuation, then, the zeroth-order effects of crystalline point defects are convolved with the partial melt effects noted earlier.

In that the low-frequency, power-law absorption behavior seems intimately related to the density, distribution and structure of interfaces (grain boundaries, solid-state phase boundaries, subgrain boundaries, ± solid-liquid phase boundaries) the interaction of lattice point defects with the structural elements of these interfaces is of critical importance to a quantitative understanding of attenuation. In the solid state, the robust

understanding of grain/phase boundaries to have a 2-D crystallographic structure based on dislocations (Sutton and Balluffi 1995) means that the jogs and kinks on these boundary dislocations (as well as those on the "free" lattice dislocations) contribute to the point-defect equilibrium of the system. Thus the kinetics of stress-induced motion of the extended defects is affected to first order by the extrinsic chemical condition. The interaction (in the case of ionic solids) of charged jogs and/or kinks with charged lattice point defects can either inhibit or enhance the motion of the extended defect—as well as the temperature sensitivity of that motion (cf. Maier 1994; Jamnik and Raj 1996; Chiang et al. 1997, p.155). (The case of rate inhibition is fully analogous to the elastic interactions between solute atoms and dislocations/grain boundaries in metals that results in "solid-solution strengthening" (e.g., Courtney 1990, p.173).) The phenomenological experimental record of the impact of f_{H_2O} on the kinetics of dislocation creep and on fabric development of olivine is an important example. An increase in f_{H_2O}, while lowering the effective viscosity overall, is known to effect *relative* changes in the resistance to dislocation motion of different slip systems in olivine (e.g., Mackwell et al. 1985); an increase in f_{H_2O} has also been correlated with an increase the mobility of grain boundaries (e.g., Jung and Karato 2001a). The combination of the two f_{H_2O} effects, in the presence of a constant deviatoric stress, has been demonstrated to result in distinctly different fabric (i.e., lattice preferred orientation) for the deformed material compared to that seen for nominally "dry" conditions (Jung and Karato 2001b). The impact on seismic responses are (i) to change significantly the wave velocity anisotropy, that is, its directionality relative to the principal stress directions, and (ii) to decrease the variety of grain boundary structures in the deformed material (a geometrical requirement consistent with the development of fabric), and so affect the absorption spectrum (cf. the case for the β-In_3Sn creep specimens presented in Fig. 13b, where one aspect of fabric—spatial distribution of low-angle boundary structures—has a notable, demonstrable effect on absorption).

The fabric effect presented above is based on the kinetic response of continued, accumulated strain in an polycrystalline aggregate. But, as noted earlier, the attenuation response is that associated with a very small stress pulse that adds to the overall stress potential giving rise to the large-scale deformation. Both the crystallographic structure *and* the electrostatic structure of the interfaces dictates the response: the stress-pulse-induced climb and glide of primary and secondary grain (phase)-boundary dislocations are subject both to their specific crystallography and to the electrostatic interactions with lattice point defects. The electrostatic and crystallographic structures are coupled to the extrinsic point-defect chemistry. A dramatic, and quantitatively characterized, example of the boundary-structure/extrinsic-defect relationship is the case of "twist" boundary (boundary normal and twist axis both [001]) structure in pure (BCC) α-iron and α-iron doped with 0.18 at % gold (Sickafus and Sass 1985). TEM and ion-backscattering spectroscopy proved that the impurity gold atoms preferentially segregate to the grain boundary, and the segregation results in a two-dimensional structural reaction. In pure α-iron, the boundary consists of an orthogonal array of $[\bar{1}10]$ and [110] screw dislocations; with the addition of the impurity, the boundary transforms to an orthogonal array of [010] and [100] screw dislocations. It is not a great stretch to believe that similar transformations occur in ionic solids; certainly, impurity segregation to boundaries has been well characterized in variety of oxides and other ionic compounds (e.g., Chiang et al. 1997, p.156).

The impact of these chemical-segregation effects and their possible influence on boundary structure and viscosity, etc. are now being contemplated by the experimental community. For example, very small concentrations of Ca^{2+} in olivine apparently effect a significant change in the thermal sensitivity of grain boundary diffusional creep (E_a in the

range 300–400 kJ mol^{-1} for aggregates prepared from pulverized San Carlos peridot, with CaO content of ~0.05 wt %; E_a in the range 600–700 kJ mol^{-1} for aggregates prepared either from a dunite with a CaO content of ~0.3-0.6 wt % or for San Carlos specimens prepared with very small amounts of CaO-bearing basaltic melt). (There are copious examples of similar behavior in the ceramic materials literature, e.g., Cho et al. (1997).) Similarly, the $\eta_{ss} \propto d^2$ result for diffusional creep in fine-grained olivine at small deviatoric stress (noted in Section 7) seems consistent with a threshold effect related to the electrostatic structure(s) of the grain boundaries. And the exact impact of water-related extrinsic defects on boundary-effected absorption have yet to be characterized. Because the stresses (and strains) involved in seismic wave attenuation are so small—and the extrapolation goals for the experimental research so grand!—these chemical effects may prove of first-order importance and so require close scrutiny in future experiments.

FINAL COMMENTS

This chapter has sought specifically to be a primer on linear viscoelasticity at high temperature and low frequency, conditions characterizing wave attenuation in geological systems. The emphasis placed on appreciating viscoelastic models and their impact on thinking with regard to attenuation is to allow the reader a base for access to the literature. The geophysical problem is a difficult one: the power-law absorption spectrum is fairly non-descript; and, despite one quantitative characterization (the shear-inviscid-boundary, diffusional creep model giving rise to Fig. 9) that can forward-predict the absorption-band behavior for a finite window of thermodynamic and microstructural conditions, the overall absorption behavior of the terrestrial planets undoubtedly involves contributions of a number of serial-kinetic mechanisms (and maybe some parallel kinetic mechanisms as well), which are difficult, indeed, to isolate experimentally.

Progress in characterizing attenuation response(s) quantitatively and with predictive capability requires advancement on a number of fronts. First, there is significant need for an improved understanding of the physical processes involved in crystalline plasticity, particularly in the areas of statistical studies of dislocations and dislocation arrays, e.g., correlating phenomenological mechanical-equation-of-state approaches to plasticity with the more classical, steady-state creep and microstructural studies, and in the application of irreversible-process thermodynamics to plasticity problems in polyphase crystalline aggregates. Second, in dynamic experiments, the role of threshold phenomena will need to be studied directly. Critical for rock and mineral studies will be the multiple impacts of various chemical potentials—including, particularly, that of H_2O—on the distributions of lattice point defects and on the structure and related viscosity of grain and phase boundaries. Nevertheless, given recent experimental and theoretical advances in the mineral physics of mechanical absorption, along with the inspiration of various geodynamic models, there is reason for optimism that an experimentally calibrated, but physically based "key" can be developed that will correlate the magnitude and frequency-sensitivity of seismic wave absorption with the stresses and accumulated strains in tectonic terranes.

ACKNOWLEDGMENTS

I have been blessed with a number of graduate students—Tye Gribb, Joe Bunton, Jeff Lee and Sam Zhang—and one postdoc—Doug Green—who have pursued with me various aspects of the attenuation problem in polycrystals and partial melts; all were outstanding collaborators and I am pleased to acknowledge them for their efforts and continued friendship. The experimental wave attenuation community in geophysics is a fairly small and collegial group, from whom I have learned a great deal; in particular, periodic discussions with Ian Jackson, Shun Karato, David Kohlstedt, Brian Bonner and

Ivan Getting have proven distinctly valuable. Likewise, in the materials and mechanics community, active collaborations with Rod Lakes and Donald Stone, and periodic discussions with Rishi Raj, continue to sharpen my perspective. The attenuation research pursued in my group at Wisconsin has been funded, in part, by the National Science Foundation Division of Earth Sciences Program in Geophysics; that support is gratefully acknowledged.

REFERENCES

Anderson DL, Given JW (1982) Absorption band Q model for the Earth. J Geophys Res 87:3893-3904

Anderson DL, Minster JB (1979) The frequency dependence of Q in the Earth and implications for mantle rheology and Chandler wobble. Geophys J R Astron Soc 58:431-440

Andrade, ENDaC (1910) On the viscous flow in metals, and allied phenomena. Proc R Soc London A84: 1-12

Ashby MF (1972) Boundary defects and atomistic aspects of boundary sliding and diffusional creep. Surf Sci 31:498-542

Bai Q, Kohlstedt DL (1992a) High-temperature creep of olivine single crystals, 2. Dislocation structures. Tectonophysics 206:1-29

Bai Q, Kohlstedt DL (1992b) Substantial hydrogen solubility in olivine and implications for water storage in the mantle. Science 357:672-674

Bai Q, Mackwell SJ, Kohlstedt DL (1991) High-temperature creep of olivine single crystals, 1. Mechanical results for buffered samples. J Geophys Res 96:2441-2463

Berckhemer H, Kampfmann W, Aulbach E, Schmeling H (1982), Shear modulus and Q of forsterite and dunite near partial melting from forced-oscillation experiments. Phys Earth Planet Inter 29:30-41

Birch F (1970) Interpretations of the low velocity zone. Phys Earth Planet Inter 3:178-181

Brady JB (1995) Diffusion data for silicate minerals, glasses and liquids. *In* Mineral Physics and Crystallography: A Handbook of Physical Constants. Ahrens TJ (ed) American Geophysical Union, Washington, p 269-290

Brodt M, Cook LS, Lakes RS (1995) Apparatus for determining the properties of materials over ten decades of frequency and time: Refinements. Rev Sci Instrum 66:5292-5297

Bunton JH (2001) The impact of grain size on the shear creep and attenuation behavior of polycrystalline olivine. MS thesis, University of Wisconsin–Madison, Madison, Wisconsin

Chan WW, Sacks IS, R. Morrow R (1989) Anelasticity of the Iceland Plateau from surface wave analysis. J Geophys Res 94:5675-5688

Chiang Y-M, Birnie D III, Kingery WD (1997) Physical Ceramics: Principles for Ceramic Science and Engineering. Wiley, New York

Cho JH, Harmer MP, Chan HM, Rickman JM, Thompson AM (1997) Effect of yttrium and lanthanum on the tensile creep behavior of aluminum oxide. J Am Ceram Soc 80:1013-1017

Clarke DR (1987) On the equilibrium thickness of intergranular glass phases in ceramic materials. J Am Ceram Soc 70:15-22

Coble RL (1963) A model for boundary diffusion controlled creep in polycrystalline materials. J Appl Phys 34:1679-1682

Cook LS, Lakes RS (1995) Viscoelastic spectra of $Cd_{0.67}Mg_{0.33}$ in torsion and bending. Metall Mater Trans A 26A:2035-2039

Cooper RF (1990) Differential stress-induced melt migration: An experimental approach. J Geophys Res 95:6979-6992

Cooper RF, Kohlstedt DL (1982) Interfacial energies in the olivine-basalt system. Adv Earth Planet Sci 12:217-228

Cooper RF, Kohlstedt DL, Chyung K (1989) Solution-precipitation enhanced diffusional creep in solid-liquid aggregates which display a non-zero dihedral angle. Acta Metall 37:1759-1771

Courtney TH (1990) Mechanical Behavior of Materials. McGraw-Hill, New York

Covey-Crump SJ (1994) The application of Hart's state variable description of inelastic deformation to Carrara marble at $T < 450^{o}C$. J Geophys Res 99:19793-19808

Crossman FW, Ashby MF (1975) The non-uniform flow of polycrystals by grain boundary sliding accommodated by power-law creep. Acta Metall 23:425-440

D'Anna G, Benoit W, Vinokur VM (1997) Internal friction and dislocation collective pinning in disordered quenched solid solutions. J Appl Phys 82:5983-5990

de Kloe R, Drury MR, van Roermund HLM (2000) Evidence for stable grain boundary melt films in experimentally deformed olivine-orthopyroxene rocks. Phys Chem Minerals 27:480-494

Dooris A, Lakes RS, Myers B, Stephens N (1999) High damping indium-tin alloys. Mech Time-Depend Mater 3:305-318

Findley WN, Lai JS, Onaran K (1976) Creep and Relaxation of Nonlinear Viscoelastic Materials. North-Holland, Amsterdam (corrected and republished: Dover Publications, New York, 1989)
Frost HJ, Ashby MF (1982) Deformation Mechanism Maps: The Plasticity and Creep of Metals and Ceramics. Pergamon Press, Oxford, UK
Glover G, Sellars CM (1973) Recovery and recrystallization during high-temperature deformation of α-iron. Metall Trans 4:765-775
Green DH, Cooper RF (1993) Dilatational anelasticity in partial melts: Viscosity, attenuation and velocity dispersion. J Geophys Res 98:19807-19817
Green DH, Cooper RF, Zhang S. (1990) Attenuation spectra of olivine/basalt partial melts: Transformation of Newtonian creep response. Geophys Res Lett 17:2097-2100
Gribb TT (1992) Low-frequency attenuation in microstructurally equilibrated silicate partial melts. MS thesis, University of Wisconsin–Madison, Madison, Wisconsin
Gribb TT, Cooper RF (1995) Anelastic behavior of silicate glass-ceramics and partial melts: Migration of the amorphous phase. *In* Plastic Deformation of Ceramics. Bradt RC, Brookes CA, Routbort JL (eds) Plenum Press, New York, p 87-97
Gribb TT, Cooper RF (1998) Low-frequency shear attenuation in polycrystalline olivine: Grain boundary diffusion and the physical significance of the Andrade model for viscoelastic rheology. J Geophys Res 103:27267-27279
Gribb TT, Cooper RF (2000) The effect of an equilibrated melt phase on the shear creep and attenuation behavior of polycrystalline olivine. Geophys Res Lett 27:2341-2344
Gribb TT, Zhang S, Cooper RF (1994) Melt migration and related attenuation in equilibrated partial melts. *In* Magmatic Systems. Ryan MP (ed) Academic Press, San Diego, p19-36
Griggs DT (1967) Hydrolytic weakening of quartz and other silicates. Geophys J Roy Astron Soc 14:19-31
Gueguen Y, Darot M, Mazot P, Woirgard J (1989) Q^{-1} of forsterite single crystals. Phys Earth Planet Inter 55:254-258
Hart EW (1970) A phenomenological theory for plastic deformation of polycrystalline metals. Acta Metall 21:295-307
Hart SR (1993) Equilibrium during mantle melting: A fractal tree model. Proc Natl Acad Sci USA 90:11914-11918
Herring C (1950) Diffusional viscosity of a polycrystalline solid. J Appl Phys 21:437-445
Hirth G, Kohlstedt DL (1995) Experimental constraints on the dynamics of the partially molten upper mantle: Deformation in the diffusion creep regime. J Geophys Res 100:1981-2001
Hirth G, Kohlstedt DL (1996) Water in the oceanic upper mantle: Implications for rheology, melt extraction and the evolution of the lithosphere. Earth Planet Sci Lett 144:93-108
Hobbs BE (1981) The influence of metamorphic environment upon the deformation of minerals. Tectonophysics 78:335-383
Holtzman B, Zimmerman ME, Kohlstedt DL, Phipps Morgan J (2001) Interactions of deformation and fluid migration I: Melt segregation in the viscous regime. EOS Trans, Am Geophys Union 82:F1107
Jackson I (1993) Progress in the experimental study of seismic wave attenuation. Ann Rev Earth Planet Sci 21:375-406
Jackson I (2000) Laboratory measurement of seismic wave dispersion and attenuation: Recent progress. *In* Earth's Deep Interior: Mineral Physics and Tomography from the Atomic to the Global Scale. Karato S-i, Forte AM, Liebermann RC, Masters G, Stixrude L (eds) American Geophysical Union, Washington, p 161-179
Jackson I, Faul UF, FitzGerald JD (2001) Laboratory measurements of seismic wave attenuation in upper-mantle materials: the effect of partial melting. EOS Trans, Am Geophys Union 82:F1163
Jackson I, FitzGerald JD, Faul UF, Tan BH (2002) Grain-size sensitive seismic-wave attenuation in polycrystalline olivine. J Geophys Res (in press)
Jackson I, Paterson MS, FitzGerald JD (1992) Seismic wave dispersion and attenuation in Åheim dunite: An experimental study. Geophys J Intl 108:517-534
Jamnik J, Raj R (1996) Space-charge-controlled diffusional creep: Volume diffusion case. J Am Ceram Soc 79:193-198
Jung H, Karato S-i (2001a) Effects of water on dynamically recrystallized grain size of olivine. J Struct Geol 23:1337-1344
Jung H, Karato S-i (2001b) Water-induced fabric transitions in olivine. Science 293:1460-1463
Karato S-i (1986) Does partial melting decrease the creep strength of the upper mantle? Nature 319: 309-310
Karato S-i (1993) Importance of anelasticity in the interpretation of seismic tomography. Geophys Res Lett 20:1623-1626
Karato S-i (1995) Effect of water on seismic wave velocities in the upper mantle. Proc Japan Acad B 71:61-66

Karato S-i, Karki B (2001) Origin of lateral variation of seismic wave velocities and density in the deep mantle. J Geophys Res 106:21771-21783.

Karato S-i, Spetzler HA (1990) Defect microdynamics in minerals and solid-state mechanisms of seismic wave attenuation and velocity dispersion in the mantle. Rev Geophys 28:399-421

Karato S-i, Paterson MS, FitzGerald JD (1986) Rheology of synthetic olivine aggregates: Influence of grain size and water. J Geophys Res 91:8151-8176

Kohlstedt DL (1990) Chemical analysis of grain boundaries in an olivine-basalt aggregate using high resolution, analytical electron microscopy. *In* The Brittle Ductile Transition in Rocks: The Heard Volume. Duba AG, Durham WB, Handin JW, Wang HF (eds) American Geophysical Union, Washington, p 211-218

Kohlstedt DL, Weathers MS (1980) Deformation-induced microstructures, paleopiezometers, and differential stresses in deeply eroded fault zones. J Geophys Res 85:6269-6285

Kohlstedt DL, Keppler H, Rubie DC (1996) Solubility of water in the α, β and γ phases of $(Mg,Fe)_2SiO_4$. Contrib Mineral Petrol 123:345-357

Kê TS (1947) Experimental evidence of the viscous behavior of grain boundaries in metals. Phys Rev 71:533-546

Kê TS (1999) Fifty-year study of grain boundary relaxation. Metall Mater Trans A 30A:2267-2295

Lakes RS (1999) Viscoelastic Solids. CRC Press, Boca Raton, Florida

Lakes RS, Quackenbush J (1996) Viscoelastic behaviour in indium-tin alloys over a wide range of frequencies and times. Philos Mag Lett 74:227-232

Lerner I, Chiang S-W, Kohlstedt DL (1979) Load relaxation studies for four alkali halides. Acta Metall 27:1187-1196

Lifshits IM, Shikin VB (1965) The theory of diffusional viscous flow of polycrystalline solids. Soviet Physics-Solid State 6:2211-2218

Mackwell SJ, Kohlstedt DL (1990) Diffusion of hydrogen in olivine: Implications for water in the mantle. J Geophys Res 95:5079-5088

Mackwell SJ, Kohlstedt DL, Paterson MS (1985) The role of water in the deformation of olivine single crystals. J Geophys Res 90:1319-1333

Maier J (1994) Defect chemistry at interfaces. Solid State Ionics 70/71:43-51

Mavko GM (1980) Velocity and attenuation in partially molten rocks. J Geophys Res 85:5173-5189

Mavko GM, Nur A (1975) Melt squirt in the asthenosphere. J Geophys Res 80:1444-1448

McKenzie D (1984) The generation and compaction of partially molten rock. J Petrol 25:713-765

Mei S, Kohlstedt DL (2000) Influence of water on plastic deformation of olivine aggregates, 1. Diffusion creep regime. J Geophys Res 105:21457-21469

Molodenskiy SM, Zharkov VN (1982) Chandler wobble and frequency dependence of Q_μ of the Earth's mantle. Phys Solid Earth 18:245-254

Mosher DR, Raj R, Kossowsky (1976) Measurement of viscosity of the grain boundary phase in hot-pressed silicon nitride. J Mater Sci 11:49-53

Nabarro FRN (1948) Deformation of crystals by the motion of single ions. *In* Report of a Conference on the Strength of Solids. Physical Society of London, UK, p 75-90

Nowick AS, Berry BS (1972) Anelastic Relaxation in Crystalline Solids. Academic Press, San Diego

O'Connell RJ, Budiansky B (1978) Measures of dissipation in viscoelastic media. Geophys Res Lett 5:5-8.

Paterson MS (1976) Some current aspects of experimental rock mechanics. Philos Trans R Soc Lond A 283:163-172

Pezzotti G, Ota K, Kleebe H-J (1996) Grain boundary relaxation in high-purity silicon nitride. J Am Ceram Soc 79:2237-2246

Plookphol T (2001) Similarity and scaling properties in dislocation microstructures generated during high-temperature load relaxation and creep of rock salt and San Carlos olivine single crystals. PhD dissertation, University of Wisconsin–Madison, Madison, Wisconsin

Raj R (1975) Transient behavior of diffusion-induced creep and creep rupture. Metall Trans A 6A: 1499-1590

Raj R, Ashby MF (1971) On grain boundary sliding and diffusional creep. Metall Trans 2:1113-1127

Richter FM, McKenzie D (1984) Dynamical models for melt segregation from a deformable matrix. J Geol 92:729-740

Ricoult DL, Kohlstedt DL (1983) Structural width of low-angle grain boundaries in olivine. Phys Chem Minerals 9:133-138

Riley GN Jr, Kohlstedt DL (1991) Kinetics of melt migration in upper mantle-type rocks. Earth Planet Sci Lett 105:500-521

Romanowicz B, Durek JJ (2000) Seismological constraints on attenuation in the Earth: A review. *In* Earth's Deep Interior: Mineral Physics and Tomography from the Atomic to the Global Scale. Karato S-i,

Forte AM, Liebermann RC, Masters G, Stixrude L (eds) American Geophysical Union, Washington, p 161-179
Schmalzried H (1995) Chemical Kinetics of Solids. VCH, Weinheim, FRG
Schoeck G, Bisogni E, Shyne J (1964) The activation energy of high temperature internal friction. Acta Metall 12:1466-1468
Scott DR, Stevenson DJ (1986) Magma ascent by porous flow. J Geophys Res 91:9283-9296
Sickafus K, Sass SL (1985) Observation of a grain boundary phase transformation induced by solute segregation. J Vac Sci Tech 3:1525-1530
Simmons G, Wang HF (1971) Single Crystal Elastic Constants and Calculated Aggregate Properties: A Handbook (Second Edn). M.I.T. Press, Cambridge, Massachusetts
Smith CS (1952) Grain shapes and other metallurgical applications of topology. *In* Metal Interfaces. American Society for Metals, Cleveland, Ohio, p 65-108
Spiegelman M, Kenyon PM (1992) The requirements for chemical disequilibrium during magma migration. Earth Planet Sci Lett 109:611-620
Stevenson DJ (1986) On the role of surface tension in the migration of melts and fluids. Geophys Res Lett 13:1149-1152
Stone DS (1991) Scaling laws in dislocation creep. Acta Metall Mater 39:599-608
Sutton AP, Balluffi RW (1995) Interfaces in Crystalline Materials. Clarendon Press, Oxford, UK
Tan B, Jackson I, FitzGerald J (1997) Shear wave dispersion and attenuation in fine-grained synthetic olivine aggregates: Preliminary results. Geophys Res Lett 24:1055-1058
Tan BH, Jackson I, FitzGerald JD (2001) High-temperature viscoelasticity of fine-grained polycrystalline olivine. Phys Chem Minerals 28:641-664
Thigpen L, Hedstrom GW, Bonner BP (1983) Inversion of creep response for retardation spectra and dynamic viscoelastic functions. J Appl Mech 105:361-366
Toomey DR, Wilcock WSD, Solomon SC, Hammond WC, Orcutt JA (1998) Mantle seismic structure beneath the MELT region of the East Pacific Rise from P and S wave tomography. Science 280: 1224-1227
Twiss RJ (1977) Theory and applicability of a recrystallized grain size paleopiezometer. Pure Appl Geophys 115:227-244
Vaughan PJ, Kohlstedt DL, Waff HS (1982) Distribution of the glass phase in hot-pressed, olivine-basalt aggregates: An electron microscopy study. Contrib Mineral Petrol 81:253-261
Waff HS (1980) Effects of the gravitational field on liquid distribution in partial melts within the upper mantle. J Geophys Res 85:1815-1825
Waff HS, Bulau JR (1979) Equilibrium fluid distribution in an ultramafic partial melt under hydrostatic stress conditions. J Geophys Res 84:6109-6114
Waff HS, Faul UH (1992) Effects of crystalline anisotropy on fluid distribution in ultra mafic partial melts. J Geophys Res 97:9003-9014
Walsh JB (1969) A new analysis of attenuation in partially melted rock. J Geophys Res 74:4333-4337
Webb S, Jackson I, FitzGerald J (1999) Viscoelasticity of the titanate perovskites $CaTiO_3$ and $SrTiO_3$ at high temperature. Phys Earth Planet Inter 115:259-291
Webb SC, Forsyth DW (1998) Structure of the upper mantle under the EPR from waveform inversion of regional events. Science 280:1227-1229
Xu Y, Zimmerman ME, Kohlstedt DL (2002) Deformation behavior of partially molten mantle rocks. *In* MARGINS Theoretical and Experimental Earth Science. Karner G (ed) Columbia University Press, New York (in press)
Yan SC, Kê TS (1987) Internal friction peaks associated with the polygonization boundaries in aluminum and dilute aluminum-copper alloys. Phys Stat Solidi 104:715-721
Zener C (1941) Theory of elasticity of polycrystals with viscous grain boundaries. Phys Rev 60:906-908
Zener C (1948) Elasticity and Anelasticity of Metals. University of Chicago Press, Chicago